Clim. Past, 19, 1931–1949, 2023
https://doi.org/10.5194/cp-19-1931-2023

Climate of the Past
Open Access
EGU

Late Cenozoic sea-surface-temperature evolution of the South Atlantic Ocean

Frida S. Hoem[1], Adrián López-Quirós[2,3], Suzanna van de Lagemaat[1], Johan Etourneau[4,5], Marie-Alexandrine Sicre[6], Carlota Escutia[7], Henk Brinkhuis[1,8], Francien Peterse[1], Francesca Sangiorgi[1], and Peter K. Bijl[1]

[1]Department of Earth Science, Utrecht University, Utrecht, the Netherlands
[2]Department of Stratigraphy and Paleontology, University of Granada, Granada, Spain
[3]Department of Geoscience, iCLIMATE Centre, Aarhus University, Aarhus C, Denmark
[4]EPHE, PSL Research University, Paris, France
[5]UMR 5805 EPOC, CNRS, University of Bordeaux, Bordeaux INP, EPOC, UMR 5805, Pessac, France
[6]LOCEAN, CNRS, Sorbonne Université, Campus Pierre et Marie Curie, Paris, France
[7]IACT, CSIC, University of Granada, Granada, Spain
[8]Department of Ocean Systems Research, Royal Netherlands Institute for Sea Research (NIOZ), Texel, the Netherlands

Correspondence: Frida S. Hoem (frida.snho@gmail.com)

Received: 18 February 2023 – Discussion started: 1 March 2023
Revised: 17 August 2023 – Accepted: 23 August 2023 – Published: 13 October 2023

Abstract. At present, a strong latitudinal sea-surface-temperature (SST) gradient of ∼16 °C exists across the Southern Ocean, maintained by the Antarctic Circumpolar Current (ACC) and a set of complex frontal systems. Together with the Antarctic ice masses, this system has formed one of the most important global climate regulators. The timing of the onset of the ACC system, its development towards modern-day strength and the consequences for the latitudinal SST gradient around the southern Atlantic Ocean are still uncertain. Here we present new TEX_{86} (TetraEther indeX of tetraethers consisting of 86 carbon atoms)-derived SST records from two sites located east of Drake Passage (south-western South Atlantic) to assist in better understanding two critical time intervals of prominent climate transitions during the Cenozoic: the late Eocene–early Oligocene (Ocean Drilling Program, ODP, Site 696) and Middle–Late Miocene (IODP Site U1536) transitions. Our results show temperate conditions (20–11 °C) during the first time interval, with a weaker latitudinal SST gradient (∼8 °C) across the Atlantic sector of the Southern Ocean compared to present day. We ascribe the similarity in SSTs between Sites 696 and 511 in the late Eocene–early Oligocene South Atlantic to a persistent, strong subpolar gyre circulation connecting the sites, which can only exist in the absence of a strong throughflow across the Drake Passage. Surprisingly, the southern South Atlantic record Site 696 shows comparable SSTs (∼12–14 °C) during both the earliest Oligocene oxygen isotope step (EOIS, ∼33.65 Ma) and the Miocene Climatic Optimum (MCO, ∼16.5 Ma). Apparently, maximum Oligocene Antarctic ice volume could coexist with warm ice-proximal surface ocean conditions, while at similar ocean temperatures, the Middle Miocene Antarctic ice sheet was likely reduced. Only a few Middle–Late Miocene (discontinuous) high-latitude records exist due to ice advances causing unconformities. Our low-resolution Site U1536 record of southern South Atlantic SSTs cooled to ∼5 °C during the Middle Miocene Climate Transition (MMCT, 14 Ma), making it the coldest oceanic region in the poorly recorded Antarctic realm and likely the main location for deep-water formation. The already-cold south-western South Atlantic conditions at the MMCT with relatively moderate additional cooling during the Late Miocene contrasts with the profound cooling in the lower latitudes and other sectors of the Southern Ocean due to northward expansion of the Southern Ocean frontal systems.

1 Introduction

Today, Southern Ocean surface flow is dominated by the strongest ocean surface current on Earth, the Antarctic Circumpolar Current (ACC). This wind-driven, eastward-flowing surface current is associated with strong meridional gradients in sea surface temperature (SST) ($\sim 16\,^{\circ}$C, ~ 45–60° S) and oceanographic conditions (Locarnini et al., 2018). Questions remain about the timing and nature of the development of the ACC and concomitant evolution of the complex Southern Ocean frontal systems (Fig. 1). A primary prerequisite for the existence of a strong ACC is an unobstructed latitudinal band of (deep-ocean) water (Orsi et al., 1995; Barker and Thomas, 2004; Toggweiler et al., 2006), which is largely determined by the tectonic evolution and opening of the Tasmanian Gateway as well as the Drake Passage (Huber et al., 2004).

The tectonic evolution of the Tasmanian Gateway is relatively well constrained; early southern opening of the Tasmanian Gateway started around 49–50 Ma (Huber et al., 2004; Stickley et al., 2004; Bijl et al., 2013) with a change in course of tectonic drift of Australia from the north-east to the north (Whittaker et al., 2007). Final breakup between Australia and Antarctica started around ~ 35.5 Ma, with ocean crust formation between south-western Tasmania and Wilkes Land, Antarctica, and onset of bottom-water currents around 35.5–33.5 Ma (Stickley et al., 2004; Houben et al., 2019), although the strength of this so-called "proto-ACC" during the Oligocene remains debated. New field data reconstructing SST and water properties (Bijl et al., 2018; Hartman et al., 2018; Salabarnada et al., 2018; Evangelinos et al., 2020, 2022; Sauermilch et al., 2021; Hoem et al., 2021a, b, 2022; Duncan et al., 2022; Hou et al., 2023) allow tracing of the migration of frontal systems, which may be reconducted to opening of gateways. Furthermore, high-resolution modelling exercises (England et al., 2017; O'Brien et al., 2020; Sauermilch et al., 2021; Nooteboom et al., 2022) show a large effect of the opening and depth of the Southern Ocean gateways on the Australian–Antarctic Gulf oceanographic conditions. A recent SST compilation from around the Tasmanian Gateway (Hoem et al., 2022) shows that the latitudinal SST gradient between the Subtropical Front and the Antarctic Margin progressively increased from ~ 26 Ma onwards due to cooling at Antarctic-proximal sites. Since the Tasmanian Gateway was already open, wide and deep, this Antarctic cooling may have been related to the onset of deep-ocean connections through the Drake Passage (Lyle et al., 2007; van de Lagemaat et al., 2021). The plate tectonic configuration of the Drake Passage–Scotia Sea region is more complex than that of the Tasmanian Gateway, with various oceanic basins that opened at different times, and the separation of continental fragments from southernmost South America and from the Antarctic Peninsula (Kennett, 1977; Barker and Thomas, 2004; Maldonado et al., 2006; Lagabrielle et al., 2009; Pérez et al., 2019, 2021). The timing and nature of the opening, widening and deepening of the Drake Passage have also been much debated and are placed between 50 and 16 Ma (Barker et al., 2007; Livermore et al., 2007; Eagles and Jokat, 2014; Maldonado et al., 2014; Pérez et al., 2021; van de Lagemaat et al., 2021). While some deep-ocean sedimentary records suggest that oceanographic rearrangements were possibly linked to an early Drake Passage opening (Kennett, 1977; Scher and Martin, 2006; López-Quirós et al., 2019, 2021), we lack knowledge of the long-term evolution of South Atlantic oceanographic conditions since the late Eocene. By reconstructing the development of the South Atlantic SST gradient, we can interpret phases of Antarctic cooling, strengthening of the ACC and shifts in the frontal systems. In turn, the changes in these three processes can be linked to the throughflow of surface and deep waters through the Drake Passage.

Recent drilling efforts in and around the Scotia Sea as part of International Ocean Discovery Program (IODP) Expedition 382 (Weber et al., 2021a) and a revisit of previously drilled records in the Weddell Sea during Ocean Drilling Program (ODP) Leg 113 offer improved spatial coverage of sedimentary records across two prominent climate transitions, viz. (1) the Eocene–Oligocene transition (EOT, 33.7 Ma) and (2) the transition from the Miocene Climatic Optimum (MCO, ~ 16.5 Ma) to the Middle Miocene Climate Transition (MMCT, ~ 14.7–13.8 Ma) and the Late Miocene Cooling (LMC, ~ 7–5.4 Ma). Both transitions are marked by increases in benthic foraminiferal δ^{18}O, suggesting cooling and expansion of the Antarctic ice sheet (Rohling et al., 2022). Given the paucity of carbonaceous sediments in this region, typically employed for paleotemperature reconstructions, we choose here to generate lipid biomarker (TetraEther indeX of tetraethers consisting of 86 carbon atoms, TEX_{86}) proxy SST reconstructions, based on isoprenoid glycerol dialkyl glycerol tetraether (isoGDGT) distributions in sediments from the northern Weddell Sea at ODP Site 696 (late Eocene–early Oligocene) and southern Scotia Sea IODP Site U1536 (Middle–Late Miocene) (Fig. 1). We compare our findings to available TEX_{86}, alkenone unsaturation index ($U^{k'}_{37}$) and clumped-isotope-derived (Δ_{47}) SST records from the South Atlantic region (Fig. 1) for a reconstruction of paleoceanographic conditions over the late Cenozoic.

2 Material

2.1 Sedimentary drill cores

2.1.1 Site 696 lithology, age model and depositional setting

ODP Leg 113 Site 696 was drilled in the northern Weddell Sea (61°50.959′ S, 42°55.996′ W), on the South Orkney Microcontinent (Fig. 1), located south of the Southern Boundary (SBdy) Front. The site had a late Eocene paleolatitude of $\sim 67^{\circ}$ S (http://paleolatitude.org, last access: 1 Febru-

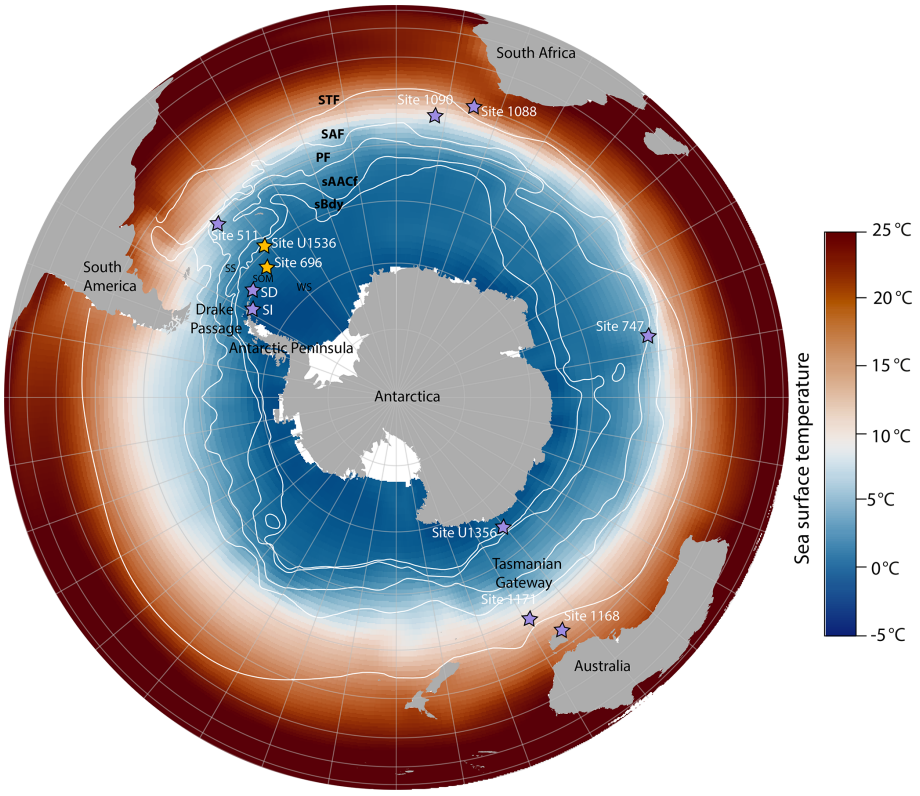

Figure 1. Present-day map of the Southern Ocean showing the location of the drill sites used in this study. Grey areas represent present-day land masses. The colours show average summer (January) SSTs from 1971–2000 (Reynolds et al., 2002). The white areas lack modern SST data, as they are covered by ice shelves. The white lines represent the smoothed, simplified position of circumpolar fronts interpreted by Orsi et al. (1995). From north to south: the Subtropical Front (STF), the Subantarctic Front (SAF), the Polar Front (PF), the Southern ACC Front (sACCf) and the Southern Boundary (SBdy) Front. SI: Seymour Island; SD: SHALLDRILL; WS: Weddell Sea; SS: Scotia Sea; SOM: South Orkney Microcontinent.

ary 2023; Version 2.1; van Hinsbergen et al., 2015, using the paleomagnetic reference frame of Torsvik et al., 2012, and the geological reconstruction of Seton et al., 2012).

Lithological descriptions and age constraints are gathered from López-Quirós et al. (2021; Fig. 2, Table S1 in the Supplement). The age model is based primarily on calcareous nannofossil biostratigraphy (Wei and Wise, 1990; Villa et al., 2008) and updated age constraints from organic walled dinoflagellate cysts (dinocysts) published previously (Houben et al., 2013, 2019; López-Quirós et al., 2021), which places the studied section of 607.6–548.9 m b.s.f. (metres below seafloor; Cores 59R–53R) at 36.0 to 33.2 Ma (Houben et al., 2013; Table S1 in the Supplement). In the sediments overlying the lower Oligocene interval, 532–529.8 m b.s.f. (Cores 52R–51R), no specific age constraint was determined, but dinocyst analysis indicates that the sediment is of Oligocene age. Core 50R was initially dated to 14.3–14.8 Ma (Barker et al., 1988; Gersonde and Burckle, 1990); however, the diatom biostratigraphic scheme was adjusted, and ages were updated to 17.6–15.4 Ma (Carter et al., 2017). More recently a thorough review of age-deterministic diatoms (*Denticulopsis maccolummii* and *Actinocyclus ingens*) have narrowed the Carter et al. (2017) age interval of Core 50R to 16.7–16.5 Ma (López-Quirós et al., 2018).

The studied sediment package at Site 696 (607.6–521.08 m b.s.f.) consists of (1) organic-rich sandy mudstone facies (607.6–606.9 m b.s.f.); (2) glaucony-bearing packstone facies (606.9 to 569.7 m b.s.f.); (3) claystone and limestone facies (569.7–548.9 m b.s.f.); (4) rhythmically interbedded sandy mudstone facies with glauconite-bearing sandstone beds (548.9–529.8 m b.s.f.); and (5) pelagic sediments, predominately biosiliceous diatom ooze (522–521 m b.s.f.) (López-Quirós et al., 2019, 2020, 2021). The glauconitic packstone beds of latest Eocene age (606.9–569.7 m b.s.f., ∼35.5–34.1 Ma) are attributed to a decline in terrigenous input to Site 696 and increased winnowing (López-Quirós et al., 2019). The glauconitic packstone beds of latest Eocene age (606.9 to 569.7 m b.s.f., ∼35.5–34.1 Ma) are attributed to a decline in terrigenous input to Site 696 and increased winnowing (López-Quirós et al., 2019) as a result of the Powell Basin at the tip of the Antarctic Peninsula opening and incipient South Orkney Microcontinent subsidence. However, the Antarctic-proximal location makes the site prone to influx of terrigenous material trans-

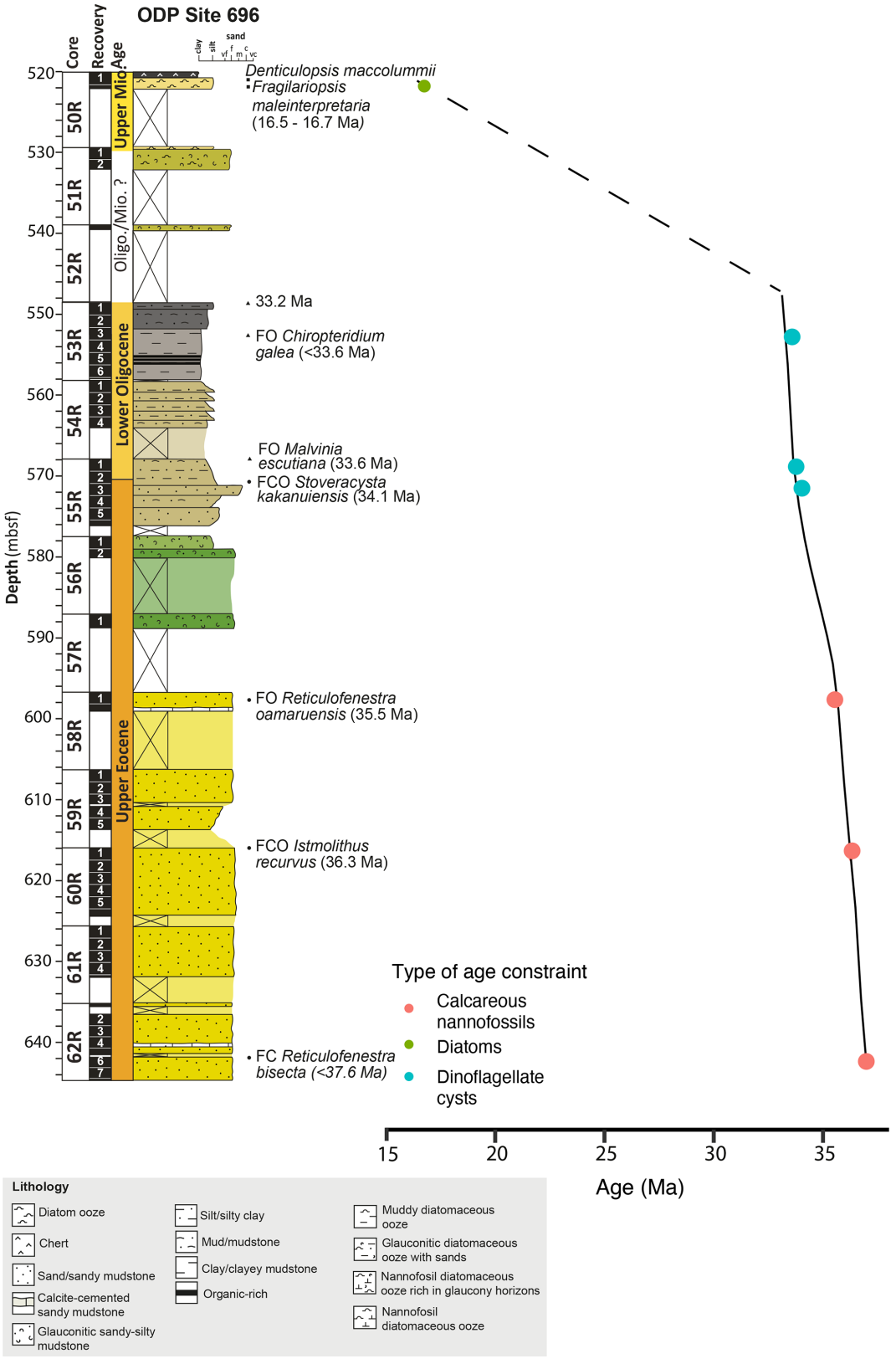

Figure 2. Age–depth model of ODP Site 696 (Table S1 in the Supplement) and lithological log modified after López-Quirós et al. (2019, 2020, 2021) and Barker et al. (1988), including new constraints of the uppermost interval (Core 50) from López-Quirós et al. (2018).

ported by icebergs, as shown by the unequivocal evidence of iceberg-rafted debris (IRD) deposited across the EOT (34.1–33.6 Ma, 576–568 m b.s.f.) at Site 696 (López-Quirós et al., 2021). Across the EOT, sediments at Site 696 reflect an increasingly distal and deeper environment as the South Orkney Microcontinent continued to deepen (López-Quirós et al., 2021). Eutrophic surface water conditions, indicative of productive and somewhat shallow-water and reduced-oxygen conditions, are indicated by dinocysts (Houben et al., 2019) and sedimentary facies (López-Quirós et al., 2019, 2021). The dominance of large-sized heterotrophic Protoperidiniacean dinocysts in the earliest Oligocene is suggested to reflect seasonal sea-ice coverage (Houben et al., 2013). During the earliest Oligocene ($\sim$ 33.6–33.2 Ma), the South Orkney Microcontinent shelf subsided, and biological production increased, partially driven by upwelling along the shelf (López-Quirós et al., 2021). Deposition of moderately to intensely bioturbated silty mudstones during the EOT is attributed to the continued subsidence-related deepening at Site 696 (López-Quirós et al., 2021). Above the clayey mudstones of the lowermost Oligocene (Core 53R; Fig. 2) we find rhythmically interbedded sandy mudstones with glauconite-bearing sandstone beds, a result of reworked sediments, deposited under bottom-current activity and possibly slumping (López-Quirós et al., 2020). The nature of this sediment complicates dating of this material. There is likely a break in the sedimentation (hiatus) around 529 m b.s.f. (the top part of Core 51R), with a sharp contact from glauconitic-bearing sandstone to mud-bearing diatom ooze 522–521 m b.s.f. (Core 50R), dated to $\sim$ 16.7–16.5 Ma (López-Quirós et al., 2018).

2.1.2 Site U1536: lithology, age model and depositional setting

Site U1536 is located in the Dove Basin, in the southern Scotia Sea (59°26.4608′ S, 41°3.6399′ W; 3220 m water depth). The site was drilled to study the Neogene flux of icebergs through "Iceberg Alley", the main pathway along which icebergs calved from the margin of the Antarctic ice sheet drift into the warmer waters of the ACC (Weber et al., 2021a). Today, the site is located just south of the Southern ACC Front (sACCf) and the Southern Boundary (SBdy) Front and is seasonally covered by sea ice (Fig. 1). The rotary drilling at Hole U1536E penetrated down to 643 m b.s.f.. Sediments have moderate to high core disturbance and biscuiting or brecciated core material due to the rough nature of rotary drilling and compaction of gravel-rich material. The lithology of the studied interval from Hole U1536E, 640–450 m b.s.f. (Cores 33R–13R), consists of silty clays with interbedded diatom ooze (Fig. 3), with an estimated average sedimentation rate of $\sim$ 4.3 cm kyr^{-1} (3.9–6.4 cm kyr^{-1}; Pérez et al., 2021). The shipboard bio- and magnetostratigraphic age model was used to date the sediments (Weber et al., 2021b; Table S2 in the Supplement). Sediments between 480–450 m b.s.f. (Cores 16R–13R) have an age of 6–5 Ma based on bio- and magnetostratigraphy. Diatom biostratigraphy between 548–535 m b.s.f. (Cores 24R–22R) indicates ages of 7.7–6.4 Ma. The sediment directly overlying Reflector-c (Weber et al., 2021b), at 617–570 m b.s.f. (Cores 30R–26R), has an age of 8.4 Ma (Pérez et al., 2021). The sediments below Reflector-c, at 622 m b.s.f. (Core 31R), are dated to $\sim$ 14.2 Ma, and as the lithologic contact is not recovered, Reflector-c could represent a prolonged time interval of slow sedimentation rates or non-deposition or erosion. The sparse brecciated lithology fragments in the lower cores, below Reflector-c (566 m b.s.f.), consist of lithified mudstone and gravel–conglomerate–breccia (Weber et al., 2021b; Perez et al., 2021).

3 Methods

3.1 Lipid extraction and glycerol dialkyl glycerol tetraether (GDGT) analysis

Lipid extraction of sediments from Site 696 was performed at the Laboratoire d'Océanographie et du Climat, Expérimentations et Approches Numériques (LOCEAN-Sorbonne Université, Paris, France). First, 71 sediment samples were freeze-dried and crushed to a fine powder. Total lipids were extracted from $\sim$ 9.5 to 15 g of homogenised sediment using a solvent mixture of 40 mL dichloromethane : methanol (DCM : MeOH; 3 : 1, v/v). The apolar fraction was separated from the polar lipids by passing the total lipid extract (TLE) over a silica column using 3 mL hexane as an eluent, followed by the recovery of the polar fraction by eluting with 3 mL DCM : MeOH (1 : 1, v/v). The polar lipid fractions were sent to Utrecht University for GDGT analysis. Sediment samples from Site U1536E were processed for GDGT analysis by lipid extraction at Utrecht University from 10 g of freeze-dried and manually powdered sediments using a Milestone Ethos X microwave system and adding DCM : MeOH (9 : 1, v/v). The TLEs were first filtered through a $NaSO_4$ column to remove potential remaining water and sediments. The TLEs were then separated on an activated Al_2O_3 column into apolar, ketone and polar fractions using hexane : DCM (9 : 1, v/v), hexane : DCM (1 : 1, v/v) and DCM : MeOH (1 : 1, $v : v$) as eluents, respectively. All polar fractions were dried under N_2. A known amount of C_{46} glycerol trialkyl glycerol tetraether (GTGT) standard was added to the polar fractions from Sites 696 and U1536, which were subsequently dissolved in hexane : isopropanol (99 : 1, v/v) to a concentration of $\sim$ 2 mg mL^{-1} and filtered through a 0.45 µm polytetrafluorethylene filter. After that, the dissolved polar fractions were injected and analysed by ultra-high-performance liquid chromatography–mass spectrometry (UHPLC–MS) according to the method described by Hopmans et al. (2016), using an Agilent 1260 Infinity UHPLC system coupled to an Agilent 6130 single-quadrupole mass detector at Utrecht University. Selected ion monitoring

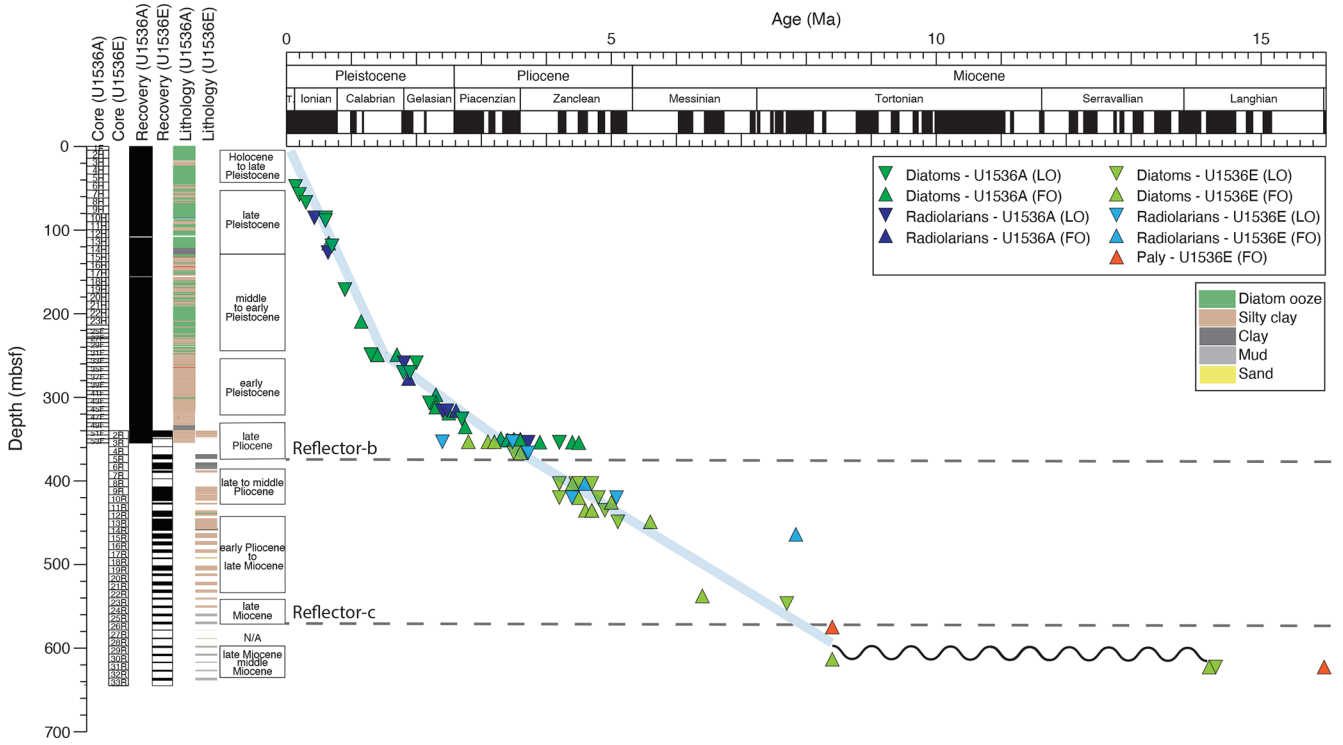

Figure 3. Site U1536 age model and lithology modified after the IODP Expedition 382 shipboard report (Weber et al., 2021b). The depth and age of the stratigraphic discontinuities (seismic reflectors) are derived from Pérez et al. (2021) (Table S2 in the Supplement; Pérez et al., 2021). LO: last occurrence; FO: first occurrence.

(SIM) was used to identify the GDGTs using their $[M+H]^+$ ions and integrated using ChemStation software. Samples with very low concentrations (i.e. peak area $<3000\,\mathrm{mV\,s^{-1}}$ and/or peak height $<3\times$ background signal) of any of the GDGTs included in the TEX_{86} were excluded from analysis.

Although lipid extractions of Sites 696 and U1536 were performed at different institutions, the latest interlaboratory comparison study (Francien Peterse, personal communication, 2023) that assessed the repeatability and reproducibility of the TEX_{86} indicates that differences in sediment extraction and workup procedures do not affect isoGDGT distributions and thus reconstructed SSTs. Instead, variations in reported TEX_{86} values appeared to be mainly introduced by the type of mass spectrometer used for GDGT analysis (Schouten et al., 2013). Since the polar fractions from both sites were analysed using the same HPLC–MS instrument at Utrecht University, the uncertainty in our TEX_{86}-based SSTs mostly represents the analytical uncertainty, which is $\pm 0.3\,^{\circ}\mathrm{C}$ based on long-term observation of the in-house standard.

3.2 GDGT indices for non-thermal overprints on TEX_{86}

The TEX_{86} SST proxy is based on the temperature dependence of the number of cyclopentane rings in GDGT membrane lipids produced by marine Thaumarchaeota and calculated as defined by Schouten et al. (2002):

$$TEX_{86} = ([\text{GDGT-2}] + [\text{GDGT-3}] + [\text{cren'}])/([\text{GDGT-1}] + [\text{GDGT-2}] + [\text{GDGT-3}] + [\text{cren'}]). \quad (1)$$

The use of TEX_{86} as a proxy for SST relies upon the assumption that isoGDGTs in marine sediments are principally derived from membrane lipids of marine pelagic Thaumarchaeota (Schouten et al., 2013). However, in some environments, non-thermal factors may alter the distribution of isoGDGTs stored in the sediment and thus the temperature signal (Supplement). We assess potential non-thermal effects on isoGDGT distributions prior to translating TEX_{86} into SSTs. We use the branched and isoprenoid tetraether (BIT) index to assess possible overprints of terrestrial GDGT input (Hopmans et al., 2004) and the fractional abundance of the crenarchaeol isomer over that of crenarchaeol to explore GDGT distribution in the sediment (fcren'; O'Brien et al., 2017), the methane index to identify contributions of methanotrophic archaea (MI; Zhang et al., 2011), the GDGT-0/crenarchaeol ratio to identify contributions of methanogenic archaea (Blaga et al., 2009), the GDGT-2/GDGT-3 ratio to assess contributions of a deep-dwelling GDGT-producing community (Taylor et al., 2013), and the Δring index to identify GDGT distributions that deviate from modern analogues (ΔRI; Zhang et al., 2016)

(Fig. S1c, panel 2–8; Fig. S2c, panel 2–8; Tables S3 and S4 in the Supplement).

3.3 TEX_{86} calibration

The empirical relationship between TEX_{86} values and SST has appeared to not always be straightforward, as reflected by continued revisions of the approach of TEX_{86}-SST calibrations (Kim et al., 2010; Tierney and Tingley, 2015; Ho and Laepple, 2016; O'Brien et al., 2017; Dunkley Jones et al., 2020). Particularly, the relationship between TEX_{86} and SST seems to become obscured at both extreme ends of the core-top calibration: at or above modern SSTs and in cold polar regions. However, for the time intervals (late Eocene–early Oligocene and Middle–Late Miocene) and locations we are targeting, we expect SSTs within the intermediate temperature range. In this study, we used the regionally varying BAYSPAR SST calibration of Tierney and Tingley (2015) to reconstruct SST (±4 °C standard calibration error) from TEX_{86} values. BAYSPAR compares measured TEX_{86} values to modern TEX_{86} values obtained from surface sediments to derive linear regression parameters and propagates uncertainties in the surface sediment data into resulting temperature predictions (Tierney and Tingley, 2015). Even when GDGT-2/GDGT-3 ratios indicate that deeper-dwelling GDGT producers do not contribute to the sedimentary signal, the GDGTs could still originate from the subsurface (50–200 m water depth) rather than the sea surface (Schouten et al., 2013). However, since the BAYSPAR calibration translates TEX_{86} values to SSTs, we refer to the proxy results as SSTs in the remainder of this work. For all new and existing TEX_{86} records discussed in this study, we applied a standard deviation of ±20 °C and a prior mean of 20 °C for the late Eocene–early Oligocene interval and 15 °C for the Miocene. We also compare the BAYSPAR-derived SST estimates with those based on the exponential function (GDGT index-2) from Kim et al. (2010) and the linear function by O'Brien et al. (2017). The SST records all show similar trends, but BAYSPAR-derived SSTs are usually cooler compared to those obtained from the functions of Kim et al. (2010) and O'Brien et al. (2017) and can thus be considered conservative estimates (Tables S3 and S4 and Figs. S3 and S4 in the Supplement).

4 Results

4.1 Site 696 GDGT distributions and TEX_{86}-SST trends

A total of 71 samples from ODP Site 696 were analysed for TEX_{86} paleothermometry (Table S3 in the Supplement). The GDGT pool consists of 90 ± 5 % isoGDGTs and 10±5 % branched GDGTs (brGDGTs), resulting in BIT index values <0.2 (Fig. 5b). The isoGDGT distributions indicate that GDGTs are primarily derived from surface-dwelling Thaumarchaeota (Fig. S1 in the Supplement). In total, nine samples had higher ΔRI values than the cutoff of 0.3 (Fig. S1b), indicating a potential non-thermal overprint on the GDGT distribution, and are excluded from SST analysis (triangles in Fig. 4). The TEX_{86}-based SST record from Site 696 (607–521 m b.s.f., 36–33 Ma and ∼ 16.5 Ma; Fig. 4) thus consists of 62 data points and predominantly ranges between 12 and 18 °C, although the total temperature range is from 4 to 25 °C (±4 °C standard calibration error). There is a general cooling trend of ∼ 8 °C between the upper Eocene and the lower Oligocene (from 20 to 12 °C between 610 and 558 m b.s.f.). This is followed by an average ∼ 5 °C increase in temperature between ∼ 558 and ∼ 552 m b.s.f.. In the organic-rich interval at ∼ 555 m b.s.f. (Core 53R, 33.5–33.2 Ma), 35 sediment samples were analysed, with 1 sample every 3 cm (∼ 15 kyr resolution). In this interval, the high-resolution TEX_{86}-SST record shows high-amplitude variability (total range of 4–21 °C, with most data points falling within the range of 8–17 °C). At ∼ 550 m b.s.f. (lower Oligocene) SSTs rapidly decrease to 10 °C. In the Middle Miocene (∼ 520 m b.s.f., $n = 2$) SST values are ∼ 14 °C.

4.2 Site U1536 GDGT distributions and TEX_{86}-SST trends

A total of 40 sediment samples from IODP Hole U1536E were processed for GDGT analysis (Table S4 in the Supplement), of which 14 had GDGT concentrations below the detection limit (Fig. 5). The Site U1536 GDGT pool consists of variable quantities of both isoGDGTs and brGDGTs, where brGDGTs are relatively more abundant in the middle (500–560 m b.s.f.) and top parts of the record (450 m b.s.f.) (Fig. S2a), resulting in high BIT index values in these intervals of the record (Fig. 5b). GDGT distributions in 12 sediment samples were outside the range of what is considered reliable for multiple indicator proxies (triangles in Figs. 5a and S2). For the remaining 14 samples TEX_{86} values were translated into SSTs using the BAYSPAR calibration (Fig. 5a). The obtained record shows temperatures of 5–11 °C for the Middle Miocene (619–640 m b.s.f.) and 1.5–5 °C for the Upper Miocene (570–450 m b.s.f.).

5 Discussion

5.1 Late Eocene–early Oligocene South Atlantic SST conditions

We have compiled available South Atlantic SST records from Site 1090 (Liu et al., 2009), Site 511 (Houben et al., 2019) and Seymour Island (Douglas et al., 2014), in addition to our new SST record from Site 696 (Fig. 6), to put the SST records into a broader regional context and discuss the surface oceanographic development during the late Eocene–early Oligocene. Our SST record from Site 696 (yellow in Fig. 6a) shows warm–temperate conditions (SST range: 22–14 °C) during the latest Eocene (∼ 36.5–33.6 Ma) and on av-

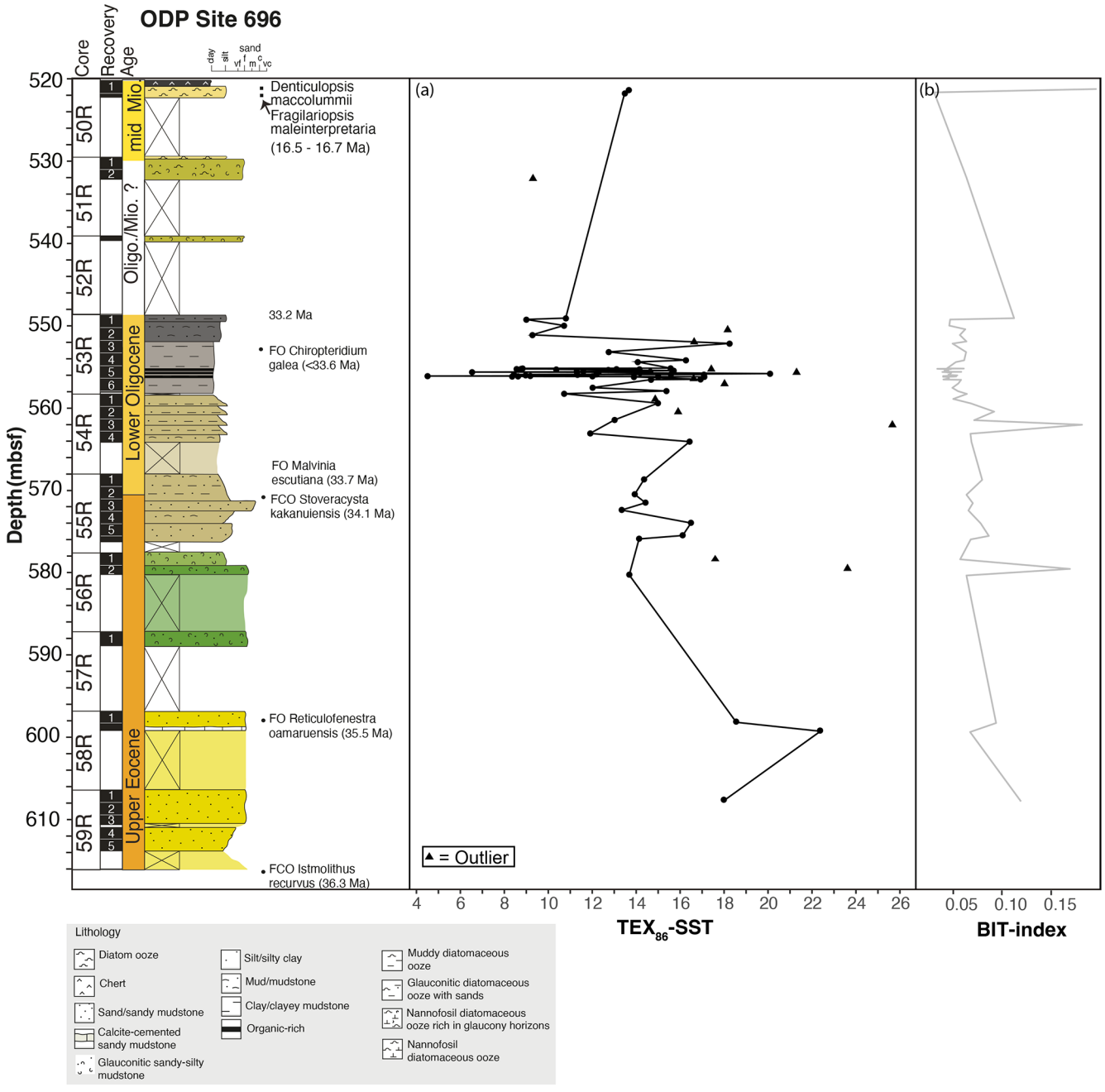

Figure 4. **(a)** TEX_{86}-SST data (BAYSPAR calibration; Tierney and Tingley, 2015). Data points marked by a triangle represent samples ($n = 9$) with a potential non-thermal overprint on the GDGT distribution (outliers; Supplement). **(b)** BIT index values (Hopmans et al., 2004) plotted next to the lithology and age constraints of Site 696, which are modified after Lopez-Quiros et al. (2021), based on Barker et al. (1988) and Lopez-Quiros et al. (2019, 2020), including new constraints of the uppermost interval (Core 50) from López-Quirós et al. (2018).

erage decreasing SSTs (∼ 15–9 °C) in the earliest Oligocene (33.6–33.2 Ma). The cooling of South Atlantic surface waters across the EOT is in broad agreement with the average Southern Ocean-wide temperature drop (Kennedy-Asser et al., 2020; Tibbett et al., 2023), the increase in benthic foraminifer $\delta^{18}O$ values as a result of deep-sea cooling, a drop in atmospheric pCO_2 levels (https://www.paleo-co2.org, last access: 1 August 2023; Pearson et al., 2009; Steinthorsdottir et al., 2016; Hoenisch, 2021; Rae et al., 2021) and the growth of a continent-wide Antarctic ice sheet across the EOT (e.g. Bohaty et al., 2012). Sites 511 and 1090 also show a stepwise cooling across the EOT (Hutchinson et al., 2021), where the first step occurs around 34.1 Ma and coincides with common IRDs at Site 696, indicating the onset of marine-terminating

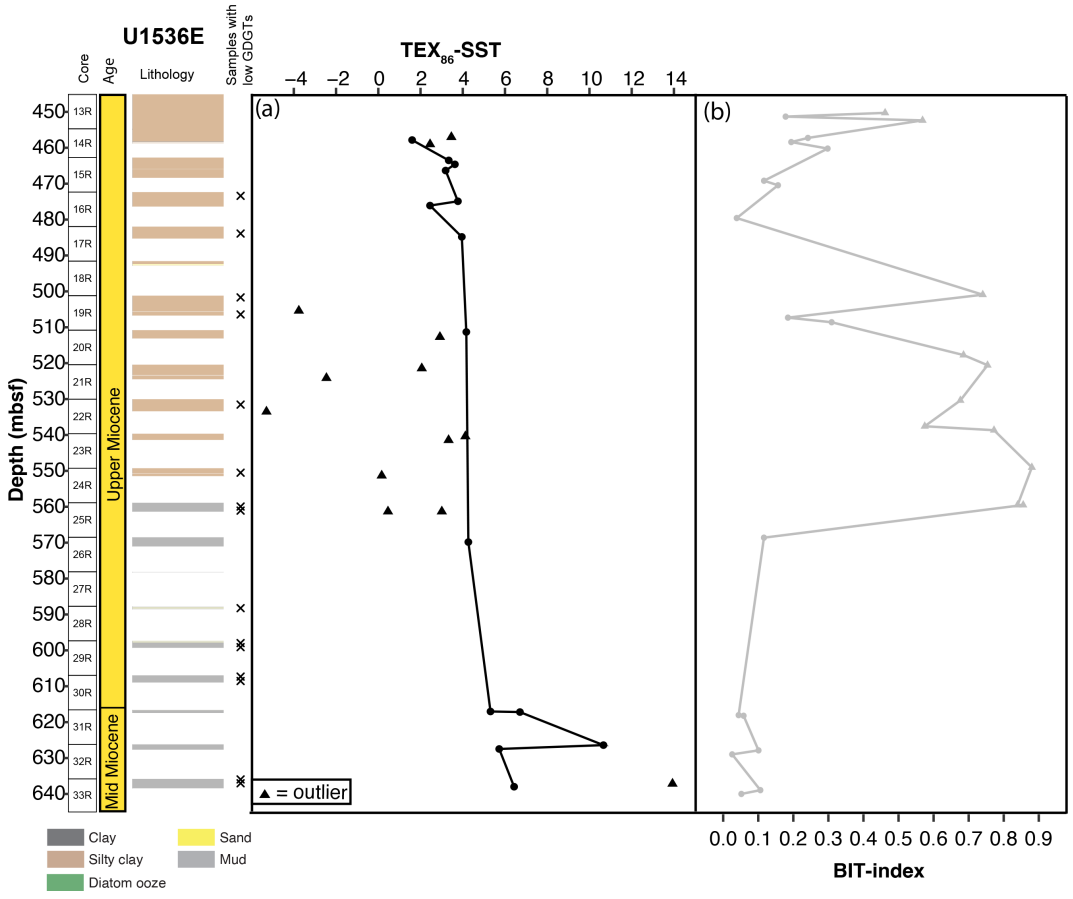

Figure 5. Biomarker indices from Site U1536. Left panel shows core recovery, estimated age and lithological composition (Weber et al., 2021a). The crosses (X) indicate samples with GDGT concentrations below the detection threshold. **(a)** TEX_{86}-SST (BAYSPAR calibration; Tierney and Tingley, 2015). Triangles mark samples with a potential non-thermal overprint on the GDGT distribution (outliers; Supplement). **(b)** BIT index (Hopmans et al., 2004) values.

glaciers in the region (López-Quirós et al., 2021), and the second step coincides with the earliest Oligocene oxygen isotope step (EOIS, 33.65 Ma; Hutchinson et al., 2021). Miospores at Site 696, believed to be of local origin from the South Orkney Microcontinent, changed concomitantly from southern beech, *Nothofagus*-dominated vegetation to a more abundant gymnosperm and cryptogam vegetation, accompanied by a rapid rise in taxon diversity after the EOIS (∼ 33.65 Ma, 568.82 m b.s.f.; Thompson et al., 2022). This shift in vegetation to a cooler and drier climate occurred after the onset of the earliest glacial expansions (∼ 34.1 Ma). Sedimentological investigations by López-Quirós et al. (2021) for the same interval showed deepening of the South Orkney Microcontinent shelf and enhancement of biological production, possibly due to upwelling along the shelf, leading to low-oxygen conditions at the seafloor.

The high-amplitude SST variability (∼ 4–8 °C) in our TEX_{86}-SST record would suggest that this upwelling regime was strongly variable. The variability in upwelling conditions could be induced by strong fluctuating ice sheet expansion and retreat and shifts in wind patterns and ocean frontal systems. Low-resolution palynological investigations on late Eocene–early Oligocene sediments from the southern South Atlantic (Houben et al., 2019; Hoem, 2022) show a highly diverse and variable dinocyst assemblage, which includes indicative Antarctic-derived, open-ocean, temperate and high-nutrient species, respectively, and indeed infers a fluctuation in surface ocean conditions, potentially related to shifts in frontal systems and upwelling regions. Alternatively, the high variability in the TEX_{86} signal could be introduced by the input of reworked isoGDGTs. Such inputs were previously found to be high at ice-proximal sites where the onset of large-scale Antarctic glaciation across the EOT caused reworking of pre-Eocene deposits, such as, for example, Prydz Bay (Tibbett et al., 2021). However, Tibbett et al. (2021) found that this had little impact on the overall TEX_{86}-SST trend. Furthermore, we record very low BIT index values (<0.2; Table S3 in the Supplement, Fig. 4b) throughout the record, whereas Eocene sediments around Antarctica are commonly high in brGDGTs (e.g. Bijl et al., 2013) because

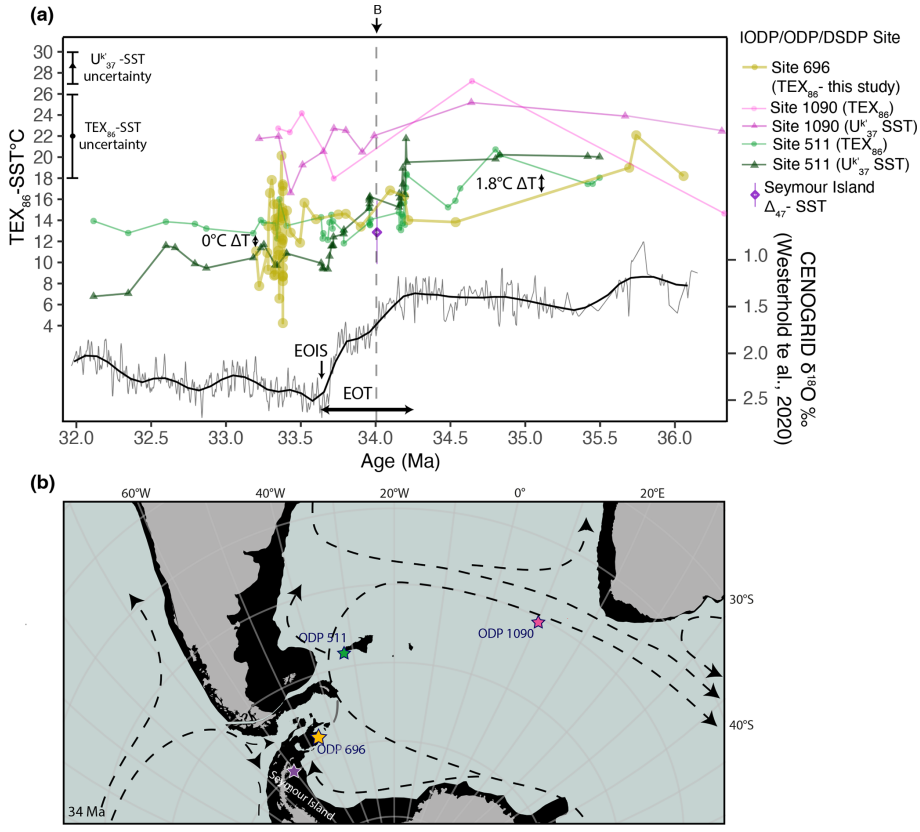

Figure 6. **(a)** The upper panel shows biomarker-based SST trends from this study (Site 696) compared with data from Site 1090 (Liu et al., 2009) and Site 511 (Houben et al., 2019) and clumped-isotope-based SST from Seymour Island (Douglas et al., 2014). The bars to the left indicate the standard calibration error in the SST proxies. The arrows indicate the temperature gradient between the TEX_{86}-SST records of Site 511 (green) and Site 696 (yellow). The lower record represents the global benthic foraminiferal $\delta^{18}O$ compilation, smoothed by a locally weighted function over 20 kyr (black curve) (CENOGRID; Westerhold et al., 2020). The black curve is the smoothed LOESS (span = 0.2). **(b)** Reconstructed paleogeographic map at 34 Ma, based on the GPlates reconstruction of van de Lagemaat et al. (2021) in the paleomagnetic reference frame of Torsvik et al. (2012). All sites from the data compilation in **(a)** are shown as stars. Arrows show the ocean circulation derived from the general circulation model (GCM) by Goldner et al. (2014).

of the well-developed soils on Antarctica at the time (Inglis et al., 2022). The lack of brGDGTs in our record thus suggests little influence of reworked Eocene GDGTs. We therefore assume that the TEX_{86} record from Site 696 represents an in situ pelagic signal and that the variability in the SST record is introduced by upwelling.

The clumped-isotope-based (Δ_{47}) SST data point from Seymour Island (34 Ma; purple star in Fig. 6b) shows a similar temperature (13 °C) to that derived from the TEX_{86} proxy at the same site (Douglas et al., 2014), as well as from nearby Site 696. The correspondence of the biomarker-derived SSTs with that from *Eurhomalea* (bivalve) Δ_{47} (mean annual temperature) adds reliability to the temperature proxies accurately reflecting SST in this region. Interestingly, the SSTs from Seymour Island and Site 696 are very similar to Site 511, even though there was a paleolatitudinal difference of ∼ 12° between Site 511 and Seymour Island (Fig. 6). The subtropical Site 1090 is the warmest site (∼ 19–27 °C) in our compilation, which is expected given its lower paleolatitude. However, the absolute SSTs of Sites 696 and 511 are strikingly similar across the EOT (Fig. 6a). The southwestern South Atlantic temperature gradient (between Sites 511 and 696) decreased from ∼ 1.8 °C in the late Eocene to ∼ 0 °C in the early Oligocene. A larger throughflow through Drake Passage would increase the temperature gradient between Sites 696 and 511. Today both sites are separated by the strong ACC and an SST gradient of > 7 °C (Locarnini et al., 2018). We therefore imply that the throughflow changes induced by the opening of Drake Passage did not change the South Atlantic Ocean circulation across the EOT. Tectonic evidence suggests that the Drake Passage was narrow, with little deep-water connection from the Pacific to the Atlantic around the EOT (Livermore et al., 2007; Eagles and Jokat, 2014; van de Lagemaat et al., 2021), which may explain the lack of regional oceanographic response. Model experiments (Huber et al., 2004; Hill et al., 2013; England et al., 2017; Sauermilch et al., 2021) show that a Southern Ocean without deep gateways featured wind-driven clockwise gyres in the

South Pacific and South Indian Ocean/Atlantic Ocean basins (Fig. 6b) that would advect warm surface waters toward the Antarctic coast. Specifically, eddy-resolving ocean model simulations by Sauermilch et al. (2021) for the Eocene show that a restricted (depths <600 m) Drake Passage throughflow would sustain the subpolar gyre and lead to SSTs reaching 19 °C in the Australian–Antarctic Basin and 15–17 °C in the subpolar Pacific and Atlantic. This is very similar to our Site 696 TEX_{86}-SST EOT record (∼ 11–18 °C). We thus propose that the small differences in SSTs between Sites 511 and 696 are the result of a restricted Drake Passage during the latest Eocene–earliest Oligocene, facilitating a persistent wind-driven gyral circulation that connected the southern South Atlantic sites in our compilation.

5.2 Middle to Late Miocene

To investigate the cooling step in the Middle to Late Miocene, the new Miocene SST records from the Antarctic-proximal south-western South Atlantic Sites 696 and U1536 are compared to records from the Antarctic Peninsula (SHALDRILL II, Core 5D; Tibbett et al., 2022) and Wilkes Land (Site U1356; Sangiorgi et al., 2018). However, there is still a lack of well-constrained and overlapping records form the Southern Ocean Middle to Late Miocene due to glacial expansions and erosion causing discontinuous records. Due to the large age uncertainties and gaps in the sedimentary records of these sites (Weber et al., 2021a; Pérez et al., 2021; Bohaty et al., 2011), we present the TEX_{86}-derived SSTs as average temperatures within two broad time intervals corresponding to the age uncertainty. We also compare SST trends from the above-mentioned sites to those from the subantarctic zone: ODP Site 1171 from the south-western Pacific Ocean (Leutert et al., 2020) and Subtropical Front, ODP Site 1088 (Herbert et al., 2016) in the south-eastern Atlantic, and Site ODP 1168 west of Tasmania (Hou et al., 2023). Further, we compare our new Site U1536 SST record to clumped-isotope bottom-water temperatures (BWTs) from South Indian Ocean ODP Site 747 (Leutert et al., 2021) (Fig. 7).

The data compilation of South Atlantic SSTs (Fig. 7a) shows a 7 °C cooling between Site 696 (yellow dots, ∼ 14 ± 4 °C standard calibration error, $n = 2$) during the Miocene Climatic Optimum (MCO, ∼ 16.5 Ma) and Site U1536 (red, ∼ 7 ± 4 °C, $n = 5$) in the Middle Miocene Climate Transition (MMCT, ∼ 14.7–13.8 Ma). Both sites were located at comparable paleolatitudes (albeit with a 2.5° latitudinal difference; Fig. 8a) during the Miocene (Fig. 7b). SSTs at Wilkes Land Site U1356 were warmer (17 °C around 17 Ma) than at Site 696 (∼ 14 °C), even though Site U1356 was situated closer to the cooler East Antarctic ice sheet. Additionally, a less pronounced cooling (SST ∼ 16–12 °C) occurred across the MMCT at Site U1356 (Sangiorgi et al., 2018) than the ∼ 7 °C cooling shown in the South Atlantic low-resolution dataset. Thus, the South Atlantic sector was colder, with a likely more proximal ice mass at the onset of MMCT than the Wilkes Land Antarctic margin. There was a ∼ 6–10 °C temperature difference between the south-western South Atlantic Antarctic-proximal Sites 696 and U1536 and the subantarctic Site 1171 (south-western Pacific Ocean), with Site 1171 clumped-isotope (Δ_{47}) SSTs of 14–12 °C and TEX_{86} SSTs of 18–13 °C during MMCT (Leutert et al., 2020). This suggests a relatively strong SST gradient between the coldest Antarctic-proximal regions and the subantarctic zone in the Middle Miocene, even though the subantarctic zone was likely situated at lower paleolatitudes in the Australian–Antarctic Gulf than in the South Atlantic due to the more southerly position of Australia. The increase in the temperature gradient in the complied SST records (Fig. 7a) during the Middle Miocene indicates breakdown of the dominant gyral circulation at the early Oligocene and a subsequent strengthening of the ACC during the Middle–Late Miocene. The alkenone-based SST reconstructions for Site 1088 and TEX_{86}-based SST reconstructions for Site 1168, together representing Subtropical Front conditions, show MCO temperatures between 32–27 °C that progressively cooled during the MMCT (∼ 24–14 °C) (Hou et al., 2023). This subtropical cooling is weaker than at the Antarctic-proximal sites, which indicates that the cooling was amplified at high latitudes. The clumped-isotope (Δ_{47}) BWT record from Site 747 in the South Indian Ocean (Leutert et al., 2021) shows strikingly similar temperatures to the reconstructed SSTs at Site U1536, which may suggest that the Weddell Gyre in the south-western South Atlantic was an important region of deep-water formation in the Miocene, like today (e.g. Orsi et al., 1999), which furthermore is in line with what modelling studies suggest for the Miocene (e.g. Herold et al., 2012). The 7 °C cooling of the south-western South Atlantic between the MCO and MMCT occurs during a time of declining pCO_2 (Foster et al., 2012; Greenop et al., 2014) (Fig. 8d) and increasing benthic foraminiferal $\delta^{18}O$ (Figs. 7a and 8c), reflecting an increasingly colder climate with larger (in area) ice sheets on the Antarctic continent with oceanward expansion (Lewis et al., 2008; Shevenell et al., 2008; Holbourn et al., 2018; Levy et al., 2019; Leutert et al., 2020). Given estimates of pCO_2 decline (by 100–300 ppm; Sosdian et al., 2018; Super et al., 2018), paleoclimate sensitivity (1.5–4.5 °C per pCO_2 doubling; Martínez-Botí et al., 2015) and polar amplification factors (2–3; Holland and Bitz, 2003), the 7 °C cooling in the south-western South Atlantic records (Sites 696 and U1536) could have been completely induced by pCO_2 decline in the Middle Miocene. This also means that regional cooling was not amplified through strengthening of the ACC and destruction of the subpolar gyre, which occurred later in the Miocene (Evangelinos et al., 2022).

By the latest Miocene (∼ 6.4–5.2 Ma), temperatures at Site U1536 cooled to an average SST of 3.4 °C ($n = 8$), which matches those at SHALLDRILL II for the earliest Pliocene (5.1–4.3 Ma, average 2.8 °C, $n = 3$). The 2–5 °C SST decrease at Site U1536 between the MMCT (∼ 14 Ma) and the latest Miocene (∼ 6.4–5.2 Ma) is relatively small compared

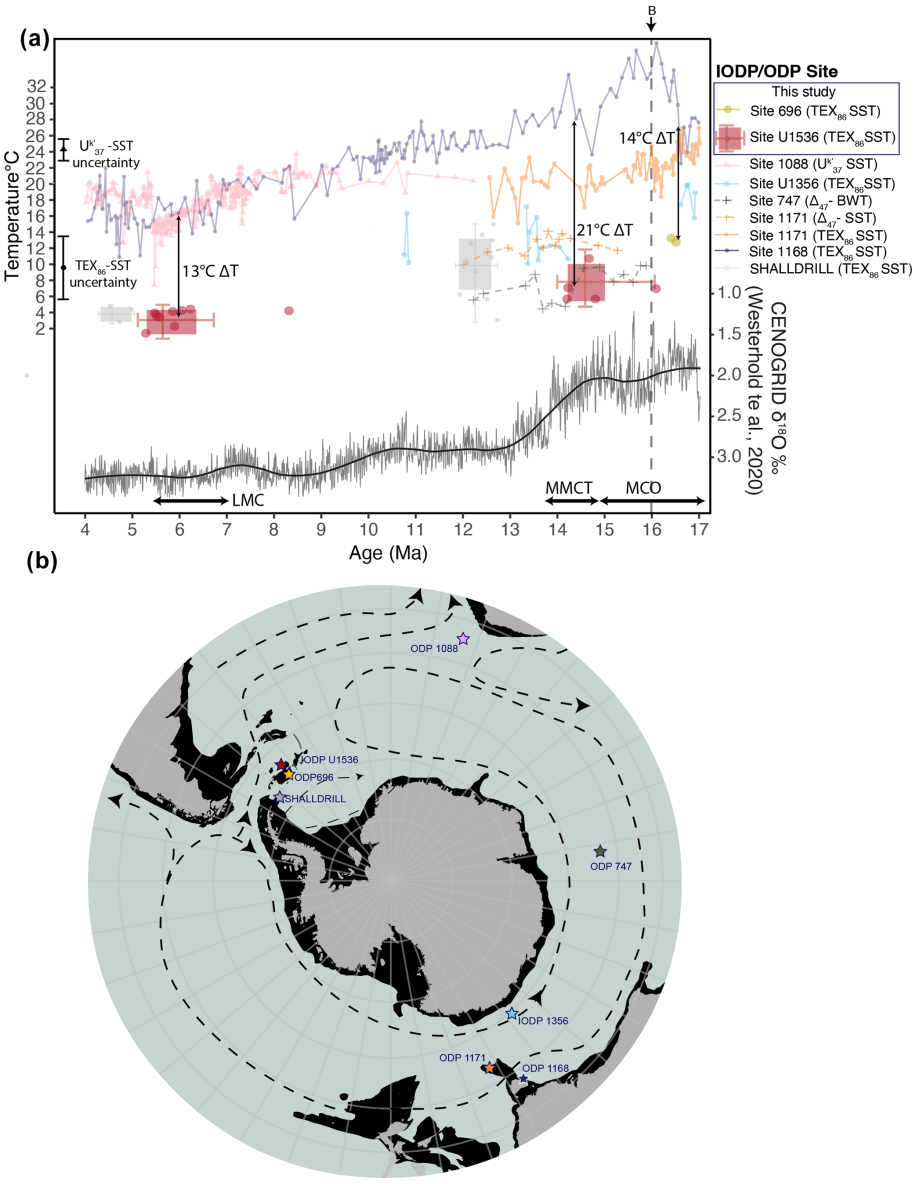

Figure 7. **(a)** TEX_{86}-based SST data from Site 696 and U1536 (this study) compared to Southern Ocean-wide SST and BWT records. The bars on the left indicate the standard calibration error in the SST proxies. Data of Site U1536 are displayed as two bar plots (red) showing the temperature ranges for the Middle Miocene (16–14 Ma) and Late Miocene (7–5.3 Ma); individual data points are shown as red dots. We compare our data to SST records from Wilkes Land Site U1356 (Sangiorgi et al., 2018), SHALDRIL II Core 5D (Tibbett et al., 2022; grey bars indicate the age uncertainty), Site 1168 (west of Tasmania; Hou et al., 2023), Site 1171 (south-western Pacific Ocean; Leutert et al., 2020), $U^{k'}_{37}$-SST data from Site 1088 (Herbert et al., 2016) and clumped-isotope bottom-water temperature (BWT) data from Leutert et al. (2021) (Site 747). The arrows indicate the temperature gradient between the TEX_{86}-SST record from the south-western South Atlantic and the Subtropical Front Site 1168. The black line is the benthic foraminiferal $\delta^{18}O$ compilation, smoothed by a locally weighted function over 20 kyr (thin blue curve) (CENOGRID; Westerhold et al., 2020). The thick black curve is the smoothed LOESS (span = 0.2). The stippled vertical line indicates the age for the paleogeographic map below. **(b)** Paleogeographic reconstruction at 16 Ma, based on the GPlates reconstruction of van de Lagemaat et al. (2021) in the paleomagnetic reference frame of Torsvik et al. (2012). All sites from data compilation in **(a)** are shown as stars. The dashed black line represents the Miocene surface ocean currents derived from Herold et al. (2012).

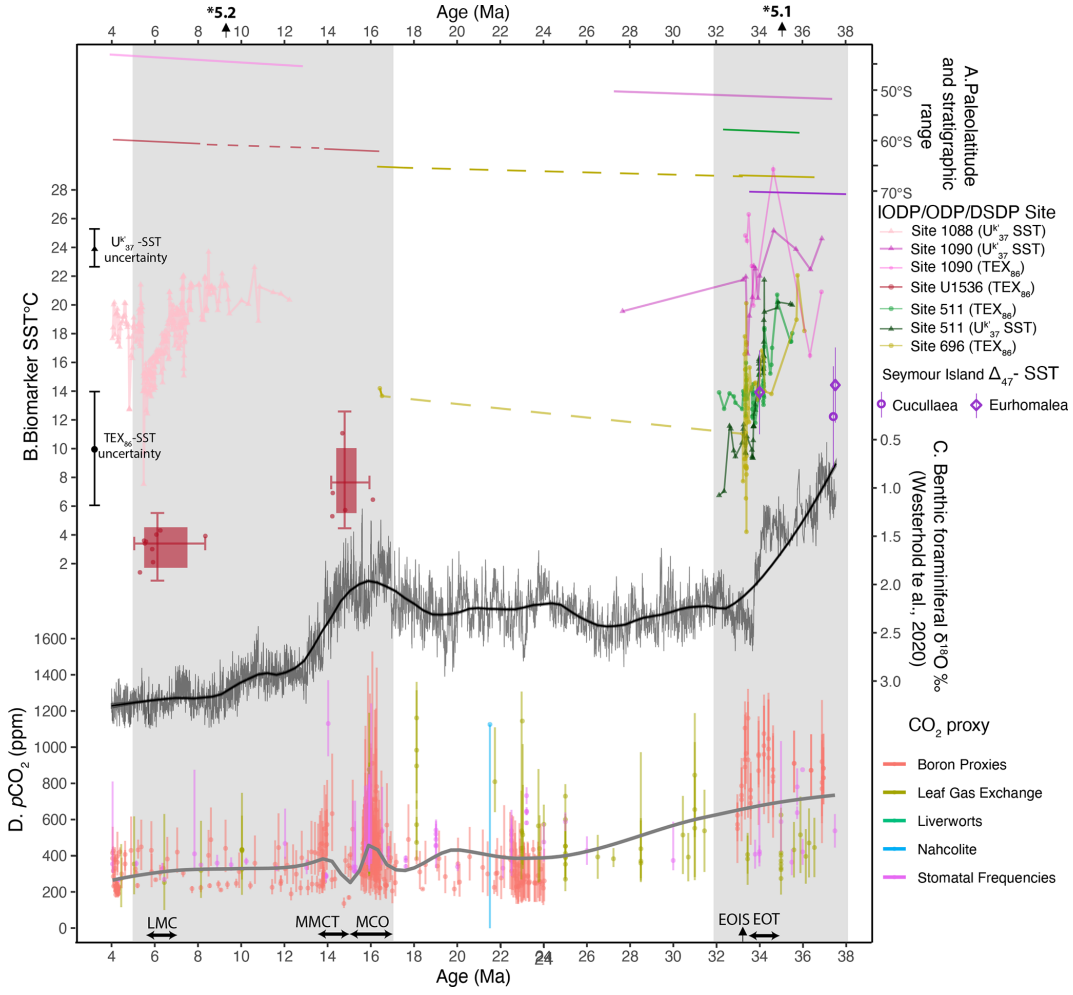

Figure 8. South Atlantic SST compilation. **(a)** Paleolatitude evolution of sites presented in this study (see legend; http://www.paleolatitude.org, last access: 1 February 2023; version 2 by van Hinsbergen et al., 2015). Stippled lines indicate hiatuses. **(b)** The coloured points and lines indicate the biomarker-based SSTs (see legend), excluding all samples with potential GDGT overprints (see Sect. 3.2). The bars on the left indicate the standard calibration error in the SST proxies. TEX_{86}-SST data from Site 696 (yellow; this study). TEX_{86}-SST data from Site 1090 (dark pink; Liu et al., 2009). $U^{k'}_{37}$-SST and TEX_{86}-SST from Site 511 (green; Houben et al., 2019). $U^{k'}_{37}$-SST from 1088 (pink; Herbert et al., 2016). TEX_{86}-SST from Site U1536 (red; this study). Clumped-isotope (Δ_{47}) SST estimates from La Meseta Fm., Seymour Island (purple; Douglas et al., 2014). **(c)** Benthic foraminiferal $\delta^{18}O$ compilation, with a locally weighted smooth over 20 kyr (black curve) (CENOGRID; Westerhold et al., 2020) and a LOESS smooth (black; span = 0.2). **(d)** Published paleo-CO_2 data from selected proxies named in the legend (https://www.paleo-co2.org, last access: 1 August 2023), with LOESS smooth (red; span = 0.3). LMC: Late Miocene Cooling; MCO: Miocene Climatic Optimum; EOIS: early Oligocene oxygen isotope step; EOT: Eocene–Oligocene transition. The shaded grey areas indicate the time intervals discussed in Sect. 5.1 and 5.2 as indicated above the figure.

to the ∼ 10 °C cooling at the Subtropical Front Sites 1168 and 1088 at the same time. We surmise that high-latitude cooling was subdued during this time interval because south-western South Atlantic surface waters (Site U1536) were already cold (5–7 °C) at the end of the MMCT (Fig. 7a) and thus could not cool as much as the subtropics. Instead, the remaining warmer part of the Southern Ocean experienced pronounced cooling during this time interval. Based on the Southern Ocean SST records (Fig. 7a), the south-western South Atlantic was already possibly the coldest region of the Southern Ocean since at least the Middle Miocene. However, there is a strong lack of Antarctic-proximal records (e.g. no records from the Ross Sea; Levy et al., 2019) that cover the MMCT to Late Miocene, partly due to glacial advances, to paint a full picture of circum-Antarctic cooling since the MMCT.

Site U1536 SSTs and Site 747 BWTs were low during the MMCT (Leutert et al., 2021), with minor cooling thereafter. Leutert et al. (2021) attributed the subdued post-MMCT cooling to the growing Antarctic ice sheet, which could have led to increased stratification and shielding of deeper waters in the Southern Ocean. We conclude here that the south-

western South Atlantic regions already reached cold conditions during the MMCT because of the proximity to ice sheets and, as a result, could not cool much more given the global cold climate of the Late Miocene. The cooling of the subtropics (Sites 1088 and 1168) is much more pronounced than the south-western South Atlantic because of the gradual northward expansion of the westerly winds, ACC and cold subantarctic waters (Leutert et al., 2020) in response to the expansion of the Antarctic ice sheet in the Late Miocene. This process likely also further promoted cooling in other sectors of the Antarctic-proximal Southern Ocean.

5.3 South Atlantic SST gradient evolution

Compiling all available SST records for the two time slices discussed above (Sect. 5.2 and 5.3) yields a unique insight into the long-term temperature trends in the South Atlantic Ocean (Fig. 8). The SST records from the South Atlantic region show unidirectional temperature drops across the EOT, with a small degree of polar amplification where Antarctic-proximal records (Site 696 and 511) cooled by $\sim 8\,^{\circ}C$ and subtropical records (Site 1090) cooled by $\sim 5\,^{\circ}C$. The strong, large and persistent South Atlantic subpolar gyre kept the latitudinal SST gradient low in the southernmost part of the South Atlantic across the EOT (Huber et al., 2004; Houben et al., 2019). The latitudinal temperature gradient in the South Atlantic increased during the MMCT (Figs. 7 and 8) due to the largest cooling at high latitudes, almost reaching modern temperatures, followed by a subdued cooling during the Late Miocene. Meanwhile the SSTs at the Subtropical Front (Sites 1090 and 1088) remained relatively stable from the earliest Oligocene (Site 1090, 33 Ma) until the Late Miocene (Site 1088) (Fig. 8), with minimal cooling until the latest Miocene.

The cooling phases in the South Atlantic across the EOT and from the MCO to the MMCT represent two climatic transitional phases, both characterised by declining atmospheric pCO_2 concentrations (Pearson et al., 2009; Foster et al., 2012; Greenop et al., 2014; Steinthorsdottir et al., 2016) and increasing benthic foraminiferal $\delta^{18}O$ values (Westerhold et al., 2020), indicating deep-sea cooling and/or ice sheet expansion (Flower and Kennett, 1993; Zachos et al., 1996) (Fig. 8). The EOT marks the first installation of a continent-wide Antarctic ice sheet (Deconto and Pollard, 2003; Coxall et al., 2005), with a volume between 60 % and 130 % of that of the present-day ice sheet (Bohaty et al., 2012). The MCO is considered to be a global warm phase, with warm–temperate ice-proximal conditions (Sangiorgi et al., 2018) and a profoundly reduced Antarctic ice volume (Shevenell et al., 2008; Foster et al., 2012), and the MMCT is a strong and stepwise transition towards a larger Antarctic ice sheet (Rohling et al., 2022). Surprisingly, although south-western South Atlantic records (Sites 696 and U1536) are of low resolution with notable age uncertainties, they do suggest similar Antarctic-proximal SSTs (~ 12–$14\,^{\circ}C$) for the early Oligocene, when a large, predominately terrestrial ice sheet with marine-terminating glaciers was installed, to those for the MCO, when ice sheets were profoundly reduced. Keeping in mind the higher-than-modern Antarctic paleotopography in the Oligocene (Wilson and Luyendyk, 2009; Duncan et al., 2022), with a gradual subsidence during the Miocene (Paxman et al., 2019), this still puts both climate phases into perspective: apparently the Oligocene Antarctic ice sheet could coexist with warm ice-proximal surface ocean conditions, while the Middle Miocene Antarctic ice sheet could be strongly reduced despite a relatively cold ice-proximal South Atlantic Ocean.

6 Conclusions

Our lipid biomarker records from IODP Site U1536 and ODP Site 696 have generated new insights for the understanding of the SST evolution of the South Atlantic Ocean, as follows:

- The EOT in the South Atlantic is characterised by a relatively small latitudinal SST gradient of $\sim 5\,^{\circ}C$ between the Subtropical Front and the western Weddell Sea and a regional decrease in SST (4–6 °C) as global pCO_2 declined.

- The South Atlantic latitudinal SST gradient remains constant across the EOT, which we ascribe to a gyral circulation that connects all South Atlantic sites and can persist in the absence of a strong throughflow through Drake Passage.

- South-western South Atlantic SSTs at the earliest Oligocene glaciation were similar to those of the warm MCO, implying that Antarctic-proximal SSTs are not the only determining factor for the extent of the Antarctic ice sheet.

- The south-western South Atlantic experienced cold polar climate conditions (SSTs of $\sim 5\,^{\circ}C$) during the MMCT. This made it the coldest oceanic region around Antarctica and the likely region of deep-water formation.

- Due to the already relatively cold conditions in the south-western South Atlantic in the Middle Miocene, it experienced little further cooling during the Late Miocene. This is in contrast to subtropical sites and other sectors of the Southern Ocean which experienced profound cooling due to northward expansion of the Southern Ocean frontal systems as the Antarctic ice sheet expanded in the Late Miocene.

Data availability. The data are available for download from the Zenodo data archive at https://doi.org/10.5281/zenodo.8279466 (Hoem et al., 2023).

Supplement. The supplement related to this article is available online at: https://doi.org/10.5194/cp-19-1931-2023-supplement.

Author contributions. FSH, PKB and FS designed the research. FSH, PKB, CE, ALQ and JE collected the samples. ALQ and CE provided depositional information, core description, facies analyses and age constraint for ODP Site 696. SvdL advised on the Drake Passage tectonic evolution and provided (paleo)geographic maps for Figs. 1, 6 and 7. JE, MAS and FSH processed samples for organic geochemistry. FSH, PKB, FP and FS interpreted the data. FSH wrote the paper with input from all authors.

Competing interests. The contact author has declared that none of the authors has any competing interests.

Disclaimer. Publisher's note: Copernicus Publications remains neutral with regard to jurisdictional claims in published maps and institutional affiliations.

Acknowledgements. This work used International Ocean Discovery Program (IODP) archived samples and data. We thank the great scientists and crew on Expedition 382, who also helped with data interpretation and discussions of results from Site U1536. We thank Mariska Hoorweg for technical support at the Utrecht University GeoLab. Frida S. Hoem and Peter K. Bijl acknowledge funding from the ERC starting grant 802835 "OceanNice". Carlota Escutia and Adrián López-Quirós acknowledge funding provided by the Spanish Ministry of Science and Innovation (grants CTM2014-60451-C2-1/2-P and CTM2017-89711-C2-1/2-P, co-funded by the European Union through FEDER funds) and JUAN DE LA CIERVA-TRAINING AID 2021 (FJC2021-047046-I, MCIN/AEI/10.13039/501100011033 and NextGenerationEU/PRTR). Suzanna van de Lagemaat acknowledges funding by NWO Vici (grant no. 865.17.001) awarded to Douwe van Hinsbergen.

Financial support. This research has been supported by the Dutch Research Council (NWO) Polar Programme (grant no. ALW.2016.001).

Review statement. This paper was edited by Ran Feng and reviewed by Xiaoqing Liu and one anonymous referee.

References

Barker, P. and Thomas, E.: Origin, signature and palaeoclimatic influence of the Antarctic Circumpolar Current, Earth-Sci. Rev., 66, 143–162, 2004.

Barker, P. F., Kennett, J. P., O'Connell, S., Berkowitz, S., Bryant, W. R., Burckle, L. H., Egeberg, P. K., Futterer, D. K., Gersonde, R. E., and Golovchenko, X.: Proceedings of the Ocean Drilling Program, Initial Reports, Vol. 113. Weddell Sea, Antarctica. Covering Leg 113 of the cruises of the drilling vessel JOIDES Resolution, Valparaiso, Chile, to East Cove, Falkland Islands, Sites 689–697, 25 December 1986–11 March 1987, https://doi.org/10.2973/odp.proc.ir.113.1988, 1988.

Barker, P. F., Filippelli, G. M., Florindo, F., Martin, E. E., and Scher, H. D.: Onset and role of the Antarctic Circumpolar Current, Deep-Sea Res. Pt. II, 54, 2388–2398, 2007.

Bijl, P. K., Bendle, J. A., Bohaty, S. M., Pross, J., Schouten, S., Tauxe, L., Stickley, C. E., McKay, R. M., Röhl, U., and Olney, M.: Eocene cooling linked to early flow across the Tasmanian Gateway, P. Natl. Acad. Sci. USA, 110, 9645–9650, 2013.

Bijl, P. K., Houben, A. J. P., Hartman, J. D., Pross, J., Salabarnada, A., Escutia, C., and Sangiorgi, F.: Paleoceanography and ice sheet variability offshore Wilkes Land, Antarctica – Part 2: Insights from Oligocene–Miocene dinoflagellate cyst assemblages, Clim. Past, 14, 1015–1033, https://doi.org/10.5194/cp-14-1015-2018, 2018.

Blaga, C. I., Reichart, G.-J., Heiri, O., and Sinninghe Damsté, J. S.: Tetraether membrane lipid distributions in water-column particulate matter and sediments: a study of 47 European lakes along a north–south transect, J. Paleolimnol., 41, 523–540, 2009.

Bohaty, S. M., Kulhanek, D. K., Wise Jr, S. W., Jemison, K., Warny, S., and Sjunneskog, C.: Age assessment of Eocene–Pliocene drill cores recovered during the SHALDRIL II expedition, Antarctic Peninsula, Tectonic, Climatic, and Cryospheric Evolution of the Antarctic Peninsula, 63–113, https://doi.org/10.1029/2010SP001049, 2011.

Bohaty, S. M., Zachos, J. C., and Delaney, M. L.: Foraminiferal Mg/Ca evidence for southern ocean cooling across the eocene–oligocene transition, Earth Planet. Sc. Lett., 317, 251–261, 2012.

Carter, A., Riley, T. R., Hillenbrand, C.-D., and Rittner, M.: Widespread Antarctic glaciation during the late Eocene, Earth Planet. Sc. Lett., 458, 49–57, 2017.

Coxall, H. K., Wilson, P. A., Pälike, H., Lear, C. H., and Backman, J.: Rapid stepwise onset of Antarctic glaciation and deeper calcite compensation in the Pacific Ocean, Nature, 433, 53–57, 2005.

DeConto, R. M. and Pollard, D.: Rapid Cenozoic glaciation of Antarctica induced by declining atmospheric CO_2, Nature, 421, 245–249, 2003.

Douglas, P. M., Affek, H. P., Ivany, L. C., Houben, A. J., Sijp, W. P., Sluijs, A., Schouten, S., and Pagani, M.: Pronounced zonal heterogeneity in Eocene southern high-latitude sea surface temperatures, P. Natl. Acad. Sci. USA, 111, 6582–6587, 2014.

Duncan, B., McKay, R., Levy, R., Naish, T., Prebble, J., Sangiorgi, F., Krishnan, S., Hoem, F., Clowes, C., and Dunkley Jones, T.: Climatic and tectonic drivers of late Oligocene Antarctic ice volume, Nat. Geosci., 15, 819–825, 2022.

Dunkley Jones, T., Eley, Y. L., Thomson, W., Greene, S. E., Mandel, I., Edgar, K., and Bendle, J. A.: OPTiMAL: a new machine learning approach for GDGT-based palaeothermometry, Clim. Past, 16, 2599–2617, https://doi.org/10.5194/cp-16-2599-2020, 2020.

Eagles, G. and Jokat, W.: Tectonic reconstructions for paleobathymetry in Drake Passage, Tectonophysics, 611, 28–50, 2014.

England, M. H., Hutchinson, D. K., Santoso, A., and Sijp, W. P.: Ice–atmosphere feedbacks dominate the response of the climate system to Drake Passage closure, J. Climate, 30, 5775–5790, https://doi.org/10.1175/JCLI-D-15-0554.1, 2017.

Evangelinos, D., Escutia, C., Etourneau, J., Hoem, F., Bijl, P., Boterblom, W., van de Flierdt, T., Valero, L., Flores, J.-A., and Rodriguez-Tovar, F. J.: Late oligocene-miocene proto-antarctic circumpolar current dynamics off the Wilkes Land margin, East Antarctica, Global Planet. Change, 191, 103221, https://doi.org/10.1016/j.gloplacha.2020.103221, 2020.

Evangelinos, D., Escutia, C., van de Flierdt, T., Valero, L., Flores, J.-A., Harwood, D. M., Hoem, F. S., Bijl, P., Etourneau, J., and Kreissig, K.: Absence of a strong, deep-reaching Antarctic Circumpolar Current zonal flow across the Tasmanian gateway during the Oligocene to early Miocene, Global Planet. Change, 208, 103718, https://doi.org/10.1016/j.gloplacha.2021.103718, 2022.

Flower, B. and Kennett, J.: Middle Miocene ocean-climate transition: High-resolution oxygen and carbon isotopic records from Deep Sea Drilling Project Site 588A, southwest Pacific, Paleoceanography, 8, 811–843, 1993.

Foster, G. L., Lear, C. H., and Rae, J. W.: The evolution of pCO_2, ice volume and climate during the middle Miocene, Earth Planet. Sc. Lett., 341, 243–254, 2012.

Gersonde, R. and Burckle, L. H.: 43. Neogene Diatom Bios15 tratigraphy of ODP LEG 113, Proceedings of the Ocean Drilling Program, Initial Reports, Vol. 113, Weddell Sea, Antarctica, Covering Leg 113 of the cruises of the drilling vessel JOIDES Resolution, Valparaiso, Chile, to East Cove, Falkland Islands, Sites 689–697, 25 December 1986–11 March 1987, https://doi.org/10.2973/odp.proc.sr.113.126.1990, 1990.

Goldner, A., Herold, N., and Huber, M.: Antarctic glaciation caused ocean circulation changes at the Eocene–Oligocene transition, Nature, 511, 574–577, 2014.

Greenop, R., Foster, G. L., Wilson, P. A., and Lear, C. H.: Middle Miocene climate instability associated with high-amplitude CO_2 variability, Paleoceanography, 29, 845–853, 2014.

Hartman, J. D., Sangiorgi, F., Salabarnada, A., Peterse, F., Houben, A. J. P., Schouten, S., Brinkhuis, H., Escutia, C., and Bijl, P. K.: Paleoceanography and ice sheet variability offshore Wilkes Land, Antarctica – Part 3: Insights from Oligocene–Miocene TEX_{86}-based sea surface temperature reconstructions, Clim. Past, 14, 1275–1297, https://doi.org/10.5194/cp-14-1275-2018, 2018.

Herbert, T. D., Lawrence, K. T., Tzanova, A., Peterson, L. C., Caballero-Gill, R., and Kelly, C. S.: Late Miocene global cooling and the rise of modern ecosystems, Nat. Geosci., 9, 843–847, https://doi.org/10.1038/Ngeo2813, 2016.

Herold, N., Huber, M., Müller, R., and Seton, M.: Modeling the Miocene climatic optimum: Ocean circulation, Paleoceanography, 27, PA1209, https://doi.org/10.1029/2010PA002041, 2012.

Hill, D. J., Haywood, A. M., Valdes, P. J., Francis, J. E., Lunt, D. J., Wade, B. S., and Bowman, V. C.: Paleogeographic controls on the onset of the Antarctic circumpolar current, Geophys. Res. Lett., 40, 5199–5204, 2013.

Ho, S. L. and Laepple, T.: Flat meridional temperature gradient in the early Eocene in the subsurface rather than surface ocean, Nat. Geosci., 9, 606–610, 2016.

Hoem, F. S.: A Song of Ice and a Warm Southern Ocean: The paleoceanographic evolution of the Oligocene–Miocene Southern Ocean, PhD thesis, vol. 260, Utrecht University, the Netherlands, https://doi.org/10.33540/1461, 2022.

Hoem, F. S., Valero, L., Evangelinos, D., Escutia, C., Duncan, B., McKay, R. M., Brinkhuis, H., Sangiorgi, F., and Bijl, P. K.: Temperate Oligocene surface ocean conditions offshore of Cape Adare, Ross Sea, Antarctica, Clim. Past, 17, 1423–1442, https://doi.org/10.5194/cp-17-1423-2021, 2021a.

Hoem, F. S., Sauermilch, I., Hou, S., Brinkhuis, H., Sangiorgi, F., and Bijl, P. K.: Late Eocene–early Miocene evolution of the southern Australian subtropical front: a marine palynological approach, J. Micropalaeontol., 40, 175–193, https://doi.org/10.5194/jm-40-175-2021, 2021b.

Hoem, F. S., Sauermilch, I., Aleksinski, A. K., Huber, M., Peterse, F., Sangiorgi, F., and Bijl, P. K.: Strength and variability of the Oligocene Southern Ocean surface temperature gradient, Communications Earth & Environment, 3, 322, https://doi.org/10.1038/s43247-022-00666-5, 2022.

Hoem, F. S., López-Quirós, A., van de Lagemaat, S., Etourneau, J., Sicre, M.-A., Escutia, C., Brinkhuis, H., Peterse, F., Sangiorgi, F., and Bijl, P. K.: Late Cenozoic Sea Surface Temperature evolution of the South Atlantic Ocean (Data sets), Zenodo [data set], https://doi.org/10.5281/zenodo.8279466, 2023.

Hoenisch, B.: Paleo-CO_2 data archive (Version 1), Zenodo [data set], https://doi.org/10.5281/zenodo.5777279, 2021.

Holbourn, A. E., Kuhnt, W., Clemens, S. C., Kochhann, K. G., Jöhnck, J., Lübbers, J., and Andersen, N.: Late Miocene climate cooling and intensification of southeast Asian winter monsoon, Nat. Commun., 9, 1584, https://doi.org/10.1038/s41467-018-03950-1, 2018.

Holland, M. M. and Bitz, C. M.: Polar amplification of climate change in coupled models, Clim. Dynam., 21, 221–232, 2003.

Hopmans, E. C., Weijers, J. W., Schefuß, E., Herfort, L., Damsté, J. S. S., and Schouten, S.: A novel proxy for terrestrial organic matter in sediments based on branched and isoprenoid tetraether lipids, Earth Planet. Sc. Lett., 224, 107–116, 2004.

Hopmans, E. C., Schouten, S., and Damsté, J. S. S.: The effect of improved chromatography on GDGT-based palaeoproxies, Org. Geochem., 93, 1–6, https://doi.org/10.1016/j.orggeochem.2015.12.006, 2016.

Hou, S., Lamprou, F., Hoem, F. S., Hadju, M. R. N., Sangiorgi, F., Peterse, F., and Bijl, P. K.: Lipid-biomarker-based sea surface temperature record offshore Tasmania over the last 23 million years, Clim. Past, 19, 787–802, https://doi.org/10.5194/cp-19-787-2023, 2023.

Houben, A. J., Bijl, P. K., Pross, J., Bohaty, S. M., Passchier, S., Stickley, C. E., Röhl, U., Sugisaki, S., Tauxe, L., and van de Flierdt, T.: Reorganization of Southern Ocean plankton ecosystem at the onset of Antarctic glaciation, Science, 340, 341–344, 2013.

Houben, A. J., Bijl, P. K., Sluijs, A., Schouten, S., and Brinkhuis, H.: Late Eocene Southern Ocean cooling and invigoration of circulation preconditioned Antarctica for full-scale glaciation, Geochem. Geophy. Geosy., 20, 2214–2234, https://doi.org/10.1029/2019GC008182, 2019.

Huber, M., Brinkhuis, H., Stickley, C. E., Döös, K., Sluijs, A., Warnaar, J., Schellenberg, S. A., and Williams, G. L.: Eocene circulation of the Southern Ocean: Was Antarctica kept warm by subtropical waters?, Paleoceanography, 19, PA4026, https://doi.org/10.1029/2004PA001014, 2004.

Hutchinson, D. K., Coxall, H. K., Lunt, D. J., Steinthorsdottir, M., de Boer, A. M., Baatsen, M., von der Heydt, A., Huber, M., Kennedy-Asser, A. T., Kunzmann, L., Ladant, J.-B., Lear, C. H., Moraweck, K., Pearson, P. N., Piga, E., Pound, M. J., Salzmann,

U., Scher, H. D., Sijp, W. P., Śliwińska, K. K., Wilson, P. A., and Zhang, Z.: The Eocene–Oligocene transition: a review of marine and terrestrial proxy data, models and model–data comparisons, Clim. Past, 17, 269–315, https://doi.org/10.5194/cp-17-269-2021, 2021.

Inglis, G. N., Toney, J. L., Zhu, J., Poulsen, C. J., Röhl, U., Jamieson, S. S., Pross, J., Cramwinckel, M. J., Krishnan, S., and Pagani, M.: Enhanced terrestrial carbon export from East Antarctica during the early Eocene, Paleoceanography and Paleoclimatology, 37, e2021PA004348, https://doi.org/10.1029/2021PA004348, 2022.

Kennedy-Asser, A. T., Lunt, D. J., Valdes, P. J., Ladant, J.-B., Frieling, J., and Lauretano, V.: Changes in the high-latitude Southern Hemisphere through the Eocene–Oligocene transition: a model–data comparison, Clim. Past, 16, 555–573, https://doi.org/10.5194/cp-16-555-2020, 2020.

Kennett, J. P.: Cenozoic evolution of Antarctic glaciation, the circum-Antarctic Ocean, and their impact on global paleoceanography, J. Geophys. Res., 82, 3843–3860, 1977.

Kim, J.-H., Van der Meer, J., Schouten, S., Helmke, P., Willmott, V., Sangiorgi, F., Koç, N., Hopmans, E. C., and Damsté, J. S. S.: New indices and calibrations derived from the distribution of crenarchaeal isoprenoid tetraether lipids: Implications for past sea surface temperature reconstructions, Geochim. Cosmochim. Ac., 74, 4639–4654, https://doi.org/10.1016/j.gca.2010.05.027, 2010.

Lagabrielle, Y., Goddéris, Y., Donnadieu, Y., Malavieille, J., and Suarez, M.: The tectonic history of Drake Passage and its possible impacts on global climate, Earth Planet. Sc. Lett., 279, 197–211, 2009.

Leutert, T. J., Auderset, A., Martínez-García, A., Modestou, S., and Meckler, A. N.: Coupled Southern Ocean cooling and Antarctic ice sheet expansion during the middle Miocene, Nat. Geosci., 13, 634–639, 2020.

Leutert, T. J., Modestou, S., Bernasconi, S. M., and Meckler, A. N.: Southern Ocean bottom-water cooling and ice sheet expansion during the middle Miocene climate transition, Clim. Past, 17, 2255–2271, https://doi.org/10.5194/cp-17-2255-2021, 2021.

Levy, R. H., Meyers, S. R., Naish, T. R., Golledge, N. R., McKay, R. M., Crampton, J. S., DeConto, R. M., De Santis, L., Florindo, F., Gasson, E. G. W., Harwood, D. M., Luyendyk, B. P., Powell, R. D., Clowes, C., and Kulhanek, D. K.: Antarctic ice-sheet sensitivity to obliquity forcing enhanced through ocean connections, Nat. Geosci., 12, 132–137, https://doi.org/10.1038/s41561-018-0284-4, 2019.

Lewis, A. R., Marchant, D. R., Ashworth, A. C., Hedenäs, L., Hemming, S. R., Johnson, J. V., Leng, M. J., Machlus, M. L., Newton, A. E., and Raine, J. I.: Mid-Miocene cooling and the extinction of tundra in continental Antarctica, P. Natl. Acad. Sci. USA, 105, 10676–10680, 2008.

Liu, Z., Pagani, M., Zinniker, D., Deconto, R., Huber, M., Brinkhuis, H., Shah, S. R., Leckie, R. M., and Pearson, A.: Global cooling during the eocene-oligocene climate transition, Science, 323, 1187–1190, https://doi.org/10.1126/science.1166368, 2009.

Livermore, R., Hillenbrand, C. D., Meredith, M., and Eagles, G.: Drake Passage and Cenozoic climate: an open and shut case?, Geochem. Geophy. Geosy., 8, Q01005, https://doi.org/10.1029/2005GC001224, 2007.

Locarnini, R. A., Mishonov, A. V., Baranova, O. K., Boyer, T. P., Zweng, M. M., Garcia, H. E., Reagan, J. R., Seidov, D., Weathers, K. W., Paver, C. R., and Smolyar, I. V.: World Ocean Atlas 2018, Volume 1: Temperature, edited by: Mishonov, A., Technical Editor, NOAA Atlas NESDIS 81, 52 pp., http://www.nodc.noaa.gov/OC5/indprod.html (last access: 1 February 2023), 2018.

López-Quirós, A., Escutia, C., Etourneau, J., Rodríguez-Tovar, F. J., Bijl, P. K., Lobo, F. J., Bohoyo, F., Evangelinos, D., and Salabarnada, A.: Eocene-Miocene paleoceanographic changes in Drake Passage (Antarctica). POLAR 2018: Where the Poles come together. Abstract Proceedings, 487, WSL Institute for Snow and Avalanche Research SLF, ISBN 978-0-948277-54-2, 2018.

López-Quirós, A., Escutia, C., Sánchez-Navas, A., Nieto, F., Garcia-Casco, A., Martín-Algarra, A., Evangelinos, D., and Salabarnada, A.: Glaucony authigenesis, maturity and alteration in the Weddell Sea: An indicator of paleoenvironmental conditions before the onset of Antarctic glaciation, Scientific Reports, 9, 13580, https://doi.org/10.1038/s41598-019-50107-1, 2019.

López-Quirós, A., Sánchez-Navas, A., Nieto, F., and Escutia, C.: New insights into the nature of glauconite, Am. Mineral., 105, 674–686, https://doi.org/10.2138/am-2020-7341, 2020.

López-Quirós, A., Escutia, C., Etourneau, J., Rodríguez-Tovar, F. J., Roignant, S., Lobo, F. J., Thompson, N., Bijl, P. K., Bohoyo, F., and Salzmann, U.: Eocene-Oligocene paleoenvironmental changes in the South Orkney Microcontinent (Antarctica) linked to the opening of Powell Basin, Global Planet. Change, 204, 103581, https://doi.org/10.1016/j.gloplacha.2021.103581, 2021.

Lyle, M., Gibbs, S., Moore, T. C., and Rea, D. K.: Late Oligocene initiation of the Antarctic Circumpolar Current: Evidence from the South Pacific, Geology, 35, 691–694, https://doi.org/10.1130/g23806a.1, 2007.

Maldonado, A., Bohoyo, F., Galindo-Zaldívar, J., Hernández-Molina, J., Jabaloy, A., Lobo, F., Rodríguez-Fernández, J., Suriñach, E., and Vázquez, J.: Ocean basins near the Scotia–Antarctic plate boundary: influence of tectonics and paleoceanography on the Cenozoic deposits, Mar. Geophys. Res., 27, 83–107, 2006.

Maldonado, A., Bohoyo, F., Galindo-Zaldívar, J., Hernández-Molina, F. J., Lobo, F. J., Lodolo, E., Martos, Y. M., Pérez, L. F., Schreider, A. A., and Somoza, L.: A model of oceanic development by ridge jumping: opening of the Scotia Sea, Global Planet. Change, 123, 152–173, 2014.

Martínez-Botí, M. A., Foster, G. L., Chalk, T. B., Rohling, E. J., Sexton, P. F., Lunt, D. J., Pancost, R. D., Badger, M. P., and Schmidt, D. N.: Plio-Pleistocene climate sensitivity evaluated using high-resolution CO_2 records, Nature, 518, 49–54, 2015.

Nooteboom, P. D., Baatsen, M., Bijl, P. K., Kliphuis, M. A., van Sebille, E., Sluijs, A., Dijkstra, H. A., and von der Heydt, A. S.: Improved Model-Data Agreement With Strongly Eddying Ocean Simulations in the Middle-Late Eocene, Paleoceanography and Paleoclimatology, 37, e2021PA004405, https://doi.org/10.1029/2021PA004405, 2022.

O'Brien, C. L., Robinson, S. A., Pancost, R. D., Damsté, J. S. S., Schouten, S., Lunt, D. J., Alsenz, H., Bornemann, A., Bottini, C., and Brassell, S. C.: Cretaceous sea-surface temperature evolution: Constraints from TEX_{86} and planktonic foraminiferal oxygen isotopes, Earth-Sci. Rev., 172, 224–247, 2017.

O'Brien, C. L., Huber, M., Thomas, E., Pagani, M., Super, J. R., Elder, L. E., and Hull, P. M.: The enigma of Oligocene climate and global surface temperature evolution, P. Natl. Acad. Sci. USA, 117, 25302–25309, 2020.

Orsi, A. H., Whitworth III, T., and Nowlin Jr., W. D.: On the meridional extent and fronts of the Antarctic Circumpolar Current, Deep-Sea Res. Pt. I, 42, 641–673, 1995.

Orsi, A. H., Johnson, G. C., and Bullister, J. L.: Circulation, mixing, and production of Antarctic Bottom Water, Prog. Oceanogr., 43, 55–109, 1999.

Paxman, G. J., Jamieson, S. S., Hochmuth, K., Gohl, K., Bentley, M. J., Leitchenkov, G., and Ferraccioli, F.: Reconstructions of Antarctic topography since the Eocene–Oligocene boundary, Palaeogeogr. Palaeocl., 535, 109346, https://doi.org/10.1016/j.palaeo.2019.109346, 2019.

Pearson, P. N., Foster, G. L., and Wade, B. S.: Atmospheric carbon dioxide through the Eocene–Oligocene climate transition, Nature, 461, 1110–1113, 2009.

Pérez, L. F., Hernández-Molina, F. J., Lodolo, E., Bohoyo, F., Galindo-Zaldívar, J., and Maldonado, A.: Oceanographic and climatic consequences of the tectonic evolution of the southern scotia sea basins, Antarctica, Earth-Sci. Rev., 198, 102922, https://doi.org/10.1016/j.earscirev.2019.102922, 2019.

Pérez, L. F., Martos, Y. M., García, M., Weber, M. E., Raymo, M. E., Williams, T., Bohoyo, F., Armbrecht, L., Bailey, I., and Brachfeld, S.: Miocene to present oceanographic variability in the Scotia Sea and Antarctic ice sheets dynamics: Insight from revised seismic-stratigraphy following IODP Expedition 382, Earth Planet. Sc. Lett., 553, 116657, https://doi.org/10.1016/j.epsl.2020.116657, 2021.

Rae, J. W., Zhang, Y. G., Liu, X., Foster, G. L., Stoll, H. M., and Whiteford, R. D.: Atmospheric CO_2 over the past 66 million years from marine archives, Annu. Rev. Earth Pl. Sc., 49, 609–641, 2021.

Reynolds, R. W., Rayner, N. A., Smith, T. M., Stokes, D. C., and Wang, W.: An improved in situ and satellite SST analysis for climate, J. Climate, 15, 1609–1625, https://doi.org/10.1175/1520-0442(2002)015<1609:Aiisas>2.0.Co;2, 2002.

Rohling, E. J., Foster, G. L., Gernon, T. M., Grant, K. M., Heslop, D., Hibbert, F. D., Roberts, A. P., and Yu, J.: Comparison and synthesis of sea-level and deep-sea temperature variations over the past 40 million years, Rev. Geophys., 60, e2022RG000775, https://doi.org/10.1029/2022RG000775, 2022.

Salabarnada, A., Escutia, C., Röhl, U., Nelson, C. H., McKay, R., Jiménez-Espejo, F. J., Bijl, P. K., Hartman, J. D., Strother, S. L., Salzmann, U., Evangelinos, D., López-Quirós, A., Flores, J. A., Sangiorgi, F., Ikehara, M., and Brinkhuis, H.: Paleoceanography and ice sheet variability offshore Wilkes Land, Antarctica – Part 1: Insights from late Oligocene astronomically paced contourite sedimentation, Clim. Past, 14, 991–1014, https://doi.org/10.5194/cp-14-991-2018, 2018.

Sangiorgi, F., Bijl, P. K., Passchier, S., Salzmann, U., Schouten, S., McKay, R., Cody, R. D., Pross, J., van de Flierdt, T., Bohaty, S. M., Levy, R., Williams, T., Escutia, C., and Brinkhuis, H.: Southern Ocean warming and Wilkes Land ice sheet retreat during the mid-Miocene, Nat. Commun., 9, 317, https://doi.org/10.1038/s41467-017-02609-7, 2018.

Sauermilch, I., Whittaker, J. M., Klocker, A., Munday, D. R., Hochmuth, K., Bijl, P. K., and LaCasce, J. H.: Gateway-driven weakening of ocean gyres leads to Southern Ocean cooling, Nat. Commun., 12, 6465, https://doi.org/10.1038/s41467-021-26658-1, 2021.

Scher, H. D. and Martin, E. E.: Timing and climatic consequences of the opening of Drake Passage, Science, 312, 428–430, 2006.

Schouten, S., Hopmans, E. C., Schefuß, E., and Damste, J. S. S.: Distributional variations in marine crenarchaeotal membrane lipids: a new tool for reconstructing ancient sea water temperatures?, Earth Planet. Sc. Lett., 204, 265–274, 2002.

Schouten, S., Hopmans, E. C., and Damsté, J. S. S.: The organic geochemistry of glycerol dialkyl glycerol tetraether lipids: A review, Org. Geochem., 54, 19–61, 2013.

Seton, M., Müller, R. D., Zahirovic, S., Gaina, C., Torsvik, T., Shephard, G., Talsma, A., Gurnis, M., Turner, M., and Maus, S.: Global continental and ocean basin reconstructions since 200 Ma, Earth-Sci. Rev., 113, 212–270, 2012.

Shevenell, A. E., Kennett, J. P., and Lea, D. W.: Middle Miocene ice sheet dynamics, deep-sea temperatures, and carbon cycling: A Southern Ocean perspective, Geochem. Geophy. Geosy., 9, Q02006, https://doi.org/10.1029/2007GC001736, 2008.

Sosdian, S. M., Greenop, R., Hain, M., Foster, G. L., Pearson, P. N., and Lear, C. H.: Constraining the evolution of Neogene ocean carbonate chemistry using the boron isotope pH proxy, Earth Planet. Sc. Lett., 498, 362–376, https://doi.org/10.1016/j.epsl.2018.06.017, 2018.

Steinthorsdottir, M., Porter, A. S., Holohan, A., Kunzmann, L., Collinson, M., and McElwain, J. C.: Fossil plant stomata indicate decreasing atmospheric CO2 prior to the Eocene–Oligocene boundary, Clim. Past, 12, 439–454, https://doi.org/10.5194/cp-12-439-2016, 2016.

Stickley, C. E., Brinkhuis, H., Schellenberg, S. A., Sluijs, A., Röhl, U., Fuller, M., Grauert, M., Huber, M., Warnaar, J., and Williams, G. L.: Timing and nature of the deepening of the Tasmanian Gateway, Paleoceanography, 19, PA4027, https://doi.org/10.1029/2004PA001022, 2004.

Super, J. R., Thomas, E., Pagani, M., Huber, M., O'Brien, C., and Hull, P. M.: North Atlantic temperature and pCO_2 coupling in the early-middle Miocene, Geology, 46, 519–522, 2018.

Taylor, K. W., Huber, M., Hollis, C. J., Hernandez-Sanchez, M. T., and Pancost, R. D.: Re-evaluating modern and Palaeogene GDGT distributions: Implications for SST reconstructions, Global Planet. Change, 108, 158–174, 2013.

Thompson, N., Salzmann, U., López-Quirós, A., Bijl, P. K., Hoem, F. S., Etourneau, J., Sicre, M.-A., Roignant, S., Hocking, E., Amoo, M., and Escutia, C.: Vegetation change across the Drake Passage region linked to late Eocene cooling and glacial disturbance after the Eocene–Oligocene transition, Clim. Past, 18, 209–232, https://doi.org/10.5194/cp-18-209-2022, 2022.

Tibbett, E. J., Scher, H. D., Warny, S., Tierney, J. E., Passchier, S., and Feakins, S. J.: Late Eocene record of hydrology and temperature from Prydz Bay, East Antarctica, Paleoceanography and Paleoclimatology, 36, e2020PA004204, https://doi.org/10.1029/2020PA004204, 2021.

Tibbett, E. J., Warny, S., Tierney, J. E., Wellner, J. S., and Feakins, S. J.: Cenozoic Antarctic Peninsula Temperatures and Glacial Erosion Signals From a Multi-Proxy Biomarker Study, Paleoceanography and Paleoclimatology, 37, e2022PA004430, https://doi.org/10.1029/2022PA004430, 2022.

Tibbett, E. J., Burls, N. J., Hutchinson, D. K., and Feakins, S. J.: Proxy-Model Comparison for the Eocene-Oligocene Transition in Southern High Latitudes, Paleoceanography and Paleoclimatology, 38, e2022PA004496, https://doi.org/10.1029/2022PA004496, 2023.

Tierney, J. E. and Tingley, M. P.: A TEX_{86} surface sediment database and extended Bayesian calibration, Scientific Data, 2, 150029, https://doi.org/10.1038/sdata.2015.29, 2015.

Toggweiler, J. R., Russell, J. L., and Carson, S. R.: Midlatitude westerlies, atmospheric CO_2, and climate change during the ice ages, Paleoceanography, 21, PA2005, https://doi.org/10.1029/2005PA001154, 2006.

Torsvik, T. H., Van der Voo, R., Preeden, U., Mac Niocaill, C., Steinberger, B., Doubrovine, P. V., Van Hinsbergen, D. J., Domeier, M., Gaina, C., and Tohver, E.: Phanerozoic polar wander, palaeogeography and dynamics, Earth-Sci. Rev., 114, 325–368, 2012.

van de Lagemaat, S. H., Swart, M. L., Vaes, B., Kosters, M. E., Boschman, L. M., Burton-Johnson, A., Bijl, P. K., Spakman, W., and van Hinsbergen, D. J.: Subduction initiation in the Scotia Sea region and opening of the Drake Passage: When and why?, Earth-Sci. Rev., 215, 103551, https://doi.org/10.1016/j.earscirev.2021.103551, 2021.

van Hinsbergen, D. J., de Groot, L. V., van Schaik, S. J., Spakman, W., Bijl, P. K., Sluijs, A., Langereis, C. G., and Brinkhuis, H.: A paleolatitude calculator for paleoclimate studies, PloS One, 10, e0126946, https://doi.org/10.1371/journal.pone.0126946, 2015.

Villa, G., Fioroni, C., Pea, L., Bohaty, S., and Persico, D.: Middle Eocene–late Oligocene climate variability: calcareous nannofossil response at Kerguelen Plateau, Site 748, Mar. Micropaleontol., 69, 173–192, 2008.

Weber, M. E., Raymo, M. E., Peck, V. L., Williams, T., and the Expedition 382 Scientists: Expedition 382 summary, Proceedings of the International Ocean Discovery Program, Volume 382, https://doi.org/10.14379/iodp.proc.382.101.2021, 2021a.

Weber, M. E., Raymo, M. E., Peck, V. L., Williams, T., and the Expedition 382 Scientists: Site U1536, Proceedings of the International Ocean Discovery Program, Volume 382, https://doi.org/10.14379/iodp.proc.382.105.2021, 2021b.

Wei, W. and Wise Jr., S. W.: Biogeographic gradients of middle Eocene-Oligocene calcareous nannoplankton in the South Atlantic Ocean, Palaeogeography, Palaeoclimatology, Palaeoecology, 79, 29–61, 1990.

Westerhold, T., Marwan, N., Drury, A. J., Liebrand, D., Agnini, C., Anagnostou, E., Barnet, J. S. K., Bohaty, S. M., De Vleeschouwer, D., Florindo, F., Frederichs, T., Hodell, D. A., Holbourn, A. E., Kroon, D., Lauretano, V., Littler, K., Lourens, L. J., Lyle, M., Palike, H., Rohl, U., Tian, J., Wilkens, R. H., Wilson, P. A., and Zachos, J. C.: An astronomically dated record of Earth's climate and its predictability over the last 66 million years, Science, 369, 1383–1387, https://doi.org/10.1126/science.aba6853, 2020.

Whittaker, J., Muller, R., Leitchenkov, G., Stagg, H., Sdrolias, M., Gaina, C., and Goncharov, A.: Major Australian-Antarctic plate reorganization at Hawaiian-Emperor bend time, Science, 318, 83–86, 2007.

Wilson, D. S. and Luyendyk, B. P.: West Antarctic paleotopography estimated at the Eocene-Oligocene climate transition, Geophys. Res. Lett., 36, L16302, https://doi.org/10.1029/2009GL039297, 2009.

Zachos, J. C., Quinn, T. M., and Salamy, K. A.: High-resolution (104 years) deep-sea foraminiferal stable isotope records of the Eocene–Oligocene climate transition, Paleoceanography, 11, 251–266, 1996.

Zhang, Y. G., Zhang, C. L. L., Liu, X. L., Li, L., Hinrichs, K. U., and Noakes, J. E.: Methane Index: A tetraether archaeal lipid biomarker indicator for detecting the instability of marine gas hydrates, Earth Planet. Sc. Lett., 307, 525–534, https://doi.org/10.1016/j.epsl.2011.05.031, 2011.

Zhang, Y. G., Pagani, M., and Wang, Z.: Ring Index: A new strategy to evaluate the integrity of TEX_{86} paleothermometry, Paleoceanography, 31, 220–232, 2016.